



This is a repository copy of *A Model of the Intrinsic Image Signal and an Evaluation of the Methodology of Intrinsic Image Signal Analysis*.

White Rose Research Online URL for this paper:
<http://eprints.whiterose.ac.uk/80348/>

Monograph:

Mayhew, J.E.W. and Zheng, Y. (1996) *A Model of the Intrinsic Image Signal and an Evaluation of the Methodology of Intrinsic Image Signal Analysis*. Research Report. ACSE Research Report 622 . Department of Automatic Control and Systems Engineering

Reuse

Unless indicated otherwise, fulltext items are protected by copyright with all rights reserved. The copyright exception in section 29 of the Copyright, Designs and Patents Act 1988 allows the making of a single copy solely for the purpose of non-commercial research or private study within the limits of fair dealing. The publisher or other rights-holder may allow further reproduction and re-use of this version - refer to the White Rose Research Online record for this item. Where records identify the publisher as the copyright holder, users can verify any specific terms of use on the publisher's website.

Takedown

If you consider content in White Rose Research Online to be in breach of UK law, please notify us by emailing eprints@whiterose.ac.uk including the URL of the record and the reason for the withdrawal request.



eprints@whiterose.ac.uk
<https://eprints.whiterose.ac.uk/>

A Model of the Intrinsic Image Signal and an Evaluation of the Methodology of Intrinsic Image Signal Analysis

J.E.W. Mayhew* and Y. Zheng#

* Artificial Intelligence Vision Research Unit

#Department of Automatic Control and Systems Engineering
University of Sheffield

Research Report No. 622

April 1996

200361612



A Model of the Intrinsic Image Signal and an Evaluation of the Methodology of Intrinsic Image Signal Analysis

J E W Mayhew* and Y Zheng#

*Artificial Intelligence Vision Research Unit

#Department of Automatic Control and Systems Engineering
University of Sheffield

Abstract

We have built a simulation to model the intrinsic signal sources. It uses estimates of parameter values derived from the published data from the optical imaging, the functional brain neuroimaging literature, and textbook physiology. The temporal dynamics of the intrinsic signals are modelled by gamma functions to give delays with the appropriate time constants. The model generates a time series representing the image intensity signal under different wavelength illumination. Perturbations that mimic systemic noise sources such as heartbeat, breathing and vasomotion can be included as desired. The simulation provides a test bed for the evaluation of the effects of different data capture regimes and methods of data analysis, and a working hypothesis of the neuro-hemo dynamics that can be used in statistical and model driven analysis of intrinsic image data. In this study we describe the simulation of an ocular dominance column mapping experiment using the methods of intrinsic imaging. We find that though accurate functional maps could be obtained using the methods of analysis in common usage in intrinsic imagery, the estimates of the resolution of the signal sources obtained did not accurately reflect the underlying parameterisation of the model. We ascribe this to the presence of the low frequency modulation of regional cerebral blood flow now known to be present in intrinsic image data, which introduces bias when the usual data capture and analysis methodology is used.

1. Introduction

1.1 Intrinsic optical imaging

Intrinsic optical imaging of neural activity is a technique which has been used for many years (Hill and Keynes 1949; Cohen 1973; Lipton 1973) Recently it has become increasingly popular as a method for investigating the functional architecture of cortex and obtaining high spatial resolution maps of cortical activity (Blasdel and Salama 1986; Grinvald, Lieke et al. 1986; Grinvald, Frostig et al. 1988). The review by Grinvald et al (1988) is an important introduction to the area. The origin of the intrinsic signal is a complex interaction of the following effects. It is generally accepted that increased neural activity produces both an increase in local blood flow and volume, a small change in the oxygen consumption, and a change in the optical transmission characteristics of neural tissue (Frostig, Lieke et al. 1990; MacVicar and Hochman 1991; Andrew and MacVicar 1994). Increased neural activity is also accompanied by an increase in glucose

consumption whether there is another component of the intrinsic signal which can be derived from this aspect of the activity is uncertain (Wray, Cope et al. 1988; Frostig, Lieke et al. 1990). The different effects interact in a complex manner to change the absorption properties of the underlying brain tissue and hence the observed spatio-temporal changes in intensity of the image data. A commonly used methodology captures images of exposed cortex under different stimulation conditions and the mean image under one condition of stimulation is subtracted from the mean image obtained under another stimulus condition to produce a differential map of cortical activity.

The magnitude of the intrinsic signals is very small and the mapping signal (the difference in change in image grey level between the preferred and orthogonal stimulus conditions say) may be of the order of less than 0.1%. Thus while overall the technique is an exciting development augmenting electro-physiological and histochemical methods for investigating brain architecture it is nevertheless sensitive to measurement and analysis artefact. Several authors have explicitly recognised the presence of vascular artefacts in intrinsic signal data (particularly surrounding the larger surface blood vessels), and have adopted various procedures to control for their influence. For example, it has sometimes been necessary to average optical images from, in some cases, hundreds or even thousands of trials to increase the signal/noise ratio. Recently Mayhew et al (1995) showed that the principal source of variability in the intrinsic signal is a pervasive low frequency (~ 0.1 Hz) oscillation in regional cerebral blood flow. This signal is present in brain parenchyma as well as the microvasculature and has many characteristics of the low frequency 'vasomotion' signals observed in peripheral microcirculation. They found concurrent measurements in brain with a laser Doppler flowmeter contained an almost identical low frequency signal. The presence of the 0.1Hz oscillation in the cerebral microcirculation could explain some of the recognised artefacts in previous intrinsic imaging studies.

1.2 Regional Cerebral Blood Flow: LDF

We refer to the low frequency oscillation in the optical intrinsic image data as the V-signal to distinguish it from the periodic oscillation in diameter of arterioles and venules. Some workers use the term 'vasomotion' to refer to this dilation and contraction of the larger vessels of the microvasculature. Laser Doppler flow (LDF) meters are frequently used in studies of regional cerebral blood flow (rCBF) e.g. (Morita, Bouskela et al. 1992; Dirnagl, Lindauer et al. 1993; Golanov and Reis 1995; Jones, Williams et al. 1995). It is worth remarking that both the optical V-signal and the LDF signal oscillation can be detected in parenchyma to a depth of 0.3-0.5 mm (possibly more depending on the illumination wavelength) as well as the more visible surface microvasculature though the LDF is 'blinded' by the signals from vessels greater than ~ 100 microns. The LDF signals are derived from the spectral broadening of the backscatter relative to the original laser illumination wavelength which is produced by moving blood cells. The amplitude of the signal (a single time series) is measured in arbitrary units (perfusion units) and confounds the number of blood cells and their velocities (for a review of the LDF technique and underlying physical principles Shepherd and Oberg (1990)). Experimental manipulations often produce changes in both the level of the DC pedestal of the signal and the amplitude

of the low frequency modulation (and the term 'rCBF' is often used to refer equally to these two aspects of the activity induced changes and frequently it seems, confounds even further, changes in flow and changes in volume). The mechanisms whereby rCBF is controlled by neural metabolic demands are still the subject of much debate and is uncertain what, if any, is the functional role of the oscillations and though it seems likely that nitric oxide is implicated at least in some manner (Iadecola 1993). Suffice it to say the presence in cortex of low frequency oscillations associated with regional blood flow is now established beyond doubt.

1.3 The V-signal: optical imagery.

Here we briefly describe the major characteristics of the V-signal. In numerous studies (Mayhew, Askew et al. 1995; Mayhew, Askew et al. 1996) we have found the signal to be present, both in the surface vasculature and parenchyma. In parenchyma we assume the V-signal derives from modulation of blood flow in the underlying capillary bed. The V-signal is not in general spatially homogenous, and it may vary both in phase, amplitude and to some extent, spectral content within an area of brain less than 2mm square. 200 micron diameter blobs completely out of phase with the surrounding area occur quite frequently in the data; as yet we have no explanation for them. The purpose of the study we describe below is to evaluate whether the presence of the V-signal in the intrinsic image data has any impact on the accuracy and reliability of the functional maps of cortical architecture when using the general data analysis methodology in common use by the intrinsic imaging community. The amplitude of the V-signal is considerably larger than the amplitude of the intrinsic signals used to obtain functional maps of cortical architecture; (it is frequently greater than 2% of the mean grey level value in contrast to ~0.1% for the mapping signals). We would expect that the V-signal would be involved in the more obvious 'vascular artefacts' commonplace in intrinsic image mapping data associated with the more visible cortical surface vasculature; but it is also possible that it could introduce bias and systematic positional errors into the maps themselves.

1.4 Project aims

To our knowledge no intrinsic imaging mapping study has systematically monitored and controlled for the V-signal. Though physiological confirmation of functional maps has been regularly obtained using data from micro-electrode recordings (Blasdel and Salama 1986; Grinvald, Lieke et al. 1986), or from cytochrome oxidase histology (Grinvald, Frostig et al. 1991; Masino, Kwon et al. 1993) little if any analysis has shown the statistical reliability of the maps per se. Thus one aim of the project is to evaluate the effect of the V-signal on the results of a simulated functional mapping experiment.

Intrinsic image data is potentially a high resolution technique for the investigation of the spatial resolution of the intrinsic signal sources. Another aim of the study is to evaluate the effects of the V-signal on the estimates of the parameters of the resolution of the intrinsic signal sources if data is collected without regard for potential biasing effects.

To this end we have implemented a model of the intrinsic signal sources using published neuroimaging data, and 'textbook' physiology. The model is used to provide a realistical test bed for the evaluation of different data capture regimes and methods of analysis. It is hoped it will serve as a working hypothesis to guide further research.

2. Modelling

In this section we describe the signal sources underlying intrinsic imagery and propose a model of the generation of the intrinsic signal image data in the context of a simulated experiment mapping the functional architecture of the ocular dominance columns in cortex.

2.1 Signal sources

Increased neural activity produces both an increase in local blood flow and volume, and a nearly commensurate increase in glucose consumption. Though as yet no optical correlate of the latter change has been described. Cytochrome aa_3 has an absorption difference spectrum but the magnitude of the absorption signal from cytochrome aa_3 is an order of magnitude smaller than hemoglobin absorption and is almost certainly dwarfed by the blood related changes (Wray, Cope et al. 1988). Focal neural activity also produces a small change in the oxygen consumption, and a change in the optical transmission characteristics of neural tissue. These effects interact in a complex manner to produce changes in intensity of the image data stream. It is thus somewhat misleading to talk of these effects as though they were causally independent but in general the volumes of HbO_2 and rHb blood and the change in transmission are regarded as the primary signal sources (Frostig, Lieke et al. 1990), and Malonek and Grinvald (1995) have proposed a temporal model of intrinsic image data of using these three sources in a simple linear additive model. Wray et al (1988) also use a linear additive model in the context of near infra red spectroscopy (NIRS), but they contrast this linearity at wavelengths greater than 700nm and with transmission spectroscopy. At wavelengths in the visible region (400-700nm) nonlinear effects are observed and furthermore, in reflection imagery the model of light transport in tissue predicts non-linearities (Zee and Delpy 1988). We enumerate below the relevant generally accepted facts that now underpin both functional brain imaging and intrinsic imaging (for reviews of both areas: Grinvald et al (1988), Bonhoeffer and Grinvald (1996), and Orrison (1995).

1) *Neural activity locally increases the volume of blood* possibly by capillary recruitment and, or alternatively, by a flow related change in the ratios of hematocrit and plasma (Orrison and Sanders 1995), the effect of this is not only to increase the volume per se but the influx of new oxygenated blood changes the proportions of the oxygenated to deoxygenated blood present in the capillary beds.

2) *Neural activity increases the flow rate* of the local blood supply (Gay, Brannan et al. 1995) Because there is only a relatively small increase in the uptake of oxygen this

increase in flow produces an increase in the saturation as the previously relatively high resting level proportion of deoxygenated blood is flushed from the capillary beds and replaced by fresh oxygenated blood.

3) *Neural activity increases oxygen consumption* producing an increase in the proportion of the reduced hemoglobin in the neighbouring microvasculature. This change in proportion may not be very large (Gay, Brannan et al. 1995).

4) *Neural activity changes the light transmission characteristics* of the underlying neural tissue (e.g. MacVicar and Hochman (1991)). Active neurons change their shape and similarly, the adjacent glia cells swell and change both their volume and that of the interstitial spaces. This has been investigated primarily *in vitro* and the effects of neural activity have been to increase the transmission characteristics of the tissue. In reflectance imagery, the generally accepted model is that the image intensity corresponding to active regions of tissue darken as a greater proportion of the incident light passes through the tissue and absorbed. However this change in the optical characteristics of the tissue will interact with the above blood related effects by changing the path length parameter in the equations relating the hemoglobin absorbance spectra to the image intensity. Thus activity induced changes in the transmission characteristics of neural tissue can change the effective volume of the sample. This is a critical confounding which will be discussed later. The issue is further complicated by findings (*in vitro*) that the sign of the transmission effect is different depending on whether the tissue was fully immersed in the bathing medium. The nature of the interface between brain tissue and bathing medium *in vivo* is undoubtedly complex but the current view is that the sign of transmittance effects is negative. Increase transmittance and the image darkens.

These physiological and physical effects interact with the wavelength of the illumination to change the image intensity measurements in a complex way. If illuminated at the isobestic wavelengths (where the absorption spectra for oxygenated and deoxygenated hemoglobin are equal), image intensity changes arise only from changes in volume and transmittance. Changes in flow rate or oxygenation cannot be detected. On the other hand, at non-isobestic illumination wavelengths, a change in the volume or in oxygen saturation will effect the image intensity. A change in flow rate can only be detected indirectly by its effects; either by changing the saturation or the volume.

In summary:

- 1) Increases in blood volume, whatever the wavelength of illumination, will result in increased absorbance and hence a darkening of the image. So, despite the fact that blood becomes 'nearly transparent' at longer wavelengths, any increase in volume will act to increase absorbance.
- 2) Under non-isobestic illumination (e.g., wavelengths between 600nm and 800nm say), an increase in the proportion of oxygenated hemoglobin acts to produce an increase in image intensity and any increase in the proportion of deoxy-hemoglobin acts to decrease the image intensity. Neural activity produces an increase in the flow of blood that exceeds the

rate of oxygen uptake. This increases the oxygen saturation and hence results in an increase in the image intensity.

3) Neural activity changes the optical properties of the tissue and results in increased transmission. This has the side effect of changing (increasing) the path length or volume parameter in the spectral absorption equations.

2.2 Assumptions and Theoretical Considerations.

We first make explicit some assumptions which we believe are fairly generally accepted and underpin the rationale of most, if not all, intrinsic imaging studies but are most clearly expressed and articulated by (Blasdel 1992; Blasdel 1992).

1. Stimulus specificity and preference is mapped to spatial structure. Though the cortex is actually a layered 3D sheet albeit thin, in the context of a single stimulus dimension it is regarded as essentially a 2D plane of patches and regions which reflect processing specificity and preferences for particular values along the stimulus dimension. The elaboration of this to account for the mapping of higher dimensional spaces onto a lower dimensional space is unnecessary here. *Spatial maps reflect functional architecture.*
2. The presentation of a stimulus, although it may produce wide spread and distributed activity, causes maximal excitation in neurons *tuned or selective* for that particular stimulus value. Furthermore, if applicable, those neurons will be minimally excited by an 'orthogonal' stimulus. Stimuli elicit preferences but, because a neuron 'prefers' stimulus A to stimulus B it does not imply that it is tuned for stimulus A. *Specificity is determined by the value of the dimension that elicits maximum activity.*
3. The presentation of a stimulus causes a spatially structured pattern of activity that at every point reflects the integrated activities of the different populations of neurons and their sensitivities to the stimulus. *Peaks of activity may not directly correspond to neural specificity.*
4. Changes in tissue reflectance and transmission characteristics are proportional to neural activity. *The greater the neural activity, the greater the magnitude of the components of the intrinsic signal source and hence the greater the changes in image intensity.*
5. The magnitude of the changes in image intensity (and hence the changes in the amplitude of the signal source) are linearly related to the amplitude of the underlying neural activity. *Patterns produced from manipulations of image data map directly to patterns of neural activity.*

Assumptions 2, 3, and 4 underpin the strategy of removing non-stimulus specific changes in activity by subtracting images from orthogonal stimulus conditions. Assumption 4 links image data to a putative neural substrate via the neural coupling to the signal sources. This and assumption 5 underpin such manipulations as the vectorial combination of activity maps from different orientation stimulation conditions to produce what are variously called angle maps (Blasdel and Salama 1986) or HLS maps (Ts'o, Frostig et al. 1990).

As mentioned above, the primary intrinsic signals are derived from oximetry and the change in the scattering properties of tissue induced by neural and glial swelling. There is a change in tissue absorption produced by activity induced oxygen uptake which increases the volume of deoxygenated hemoglobin, a more delayed and possibly much greater activity induced increase in blood flow rate (and possibly volume), which increases the volume of oxygenated blood, and a decrease in reflectance as swelling of neuronal and glial tissue increase the light transmission characteristics of the tissue. For the purposes of developing the model of the dynamics of the intrinsic image signal sources we need to make further and somewhat more detailed assumptions relating the signal sources to neural activity and the spatial distribution. We summarise briefly below some relevant facts about the intrinsic image sources.

The mechanisms coupling the blood volume related intrinsic signal sources to neural activity suggest that the signal may derive primarily from regions of neuropil rather than from neuronal cell bodies per se. Briefly, the following are well known and recently reviewed by (Jueptner and Weiller 1995).

1. Capillary density is greater in cytochrome oxidase rich 'blobs'.
2. The cytochrome oxidase (CO) rich 'blobs' are areas of abnormally high density of mitochondria and are indicators of high resting functional metabolic activity. These areas have been found to be predominantly in the neuropil.
3. Neural activity induced increase in the metabolisation of glucose has been found to occur predominantly in presynaptic axon terminals.
4. The increase in glucose uptake, being predominantly presynaptic, can arise from either excitation or inhibition.

Thus to the extent to which the intrinsic signal sources arise from changes in blood perfusion and oxygenation in capillary beds it is to be expected that these signals derive predominantly from regions of neuropil. There is evidence (Grinvald, Frostig et al. 1991; Blasdel 1992) that the CO blobs in cortex correspond to 'centres of extreme monocularity' in the intrinsic image maps of ocular dominance columns, and (Masino, Kwon et al. 1993) show a good correspondence between the intrinsic signal maps of barrel cortex and the corresponding CO histology.

The non-blood related intrinsic signal source is the change in the light scattering properties produced by tissue swelling. MacVicar and Hochman (1991) (also Andrew and MacVicar, 1994) using an *in vitro* hippocampal slice preparation found stimulation of the Shaffer collaterals produced a localised change in the transmission characteristics of the neural tissue confined to the synaptic region in stratum radiatum (neuropil) about 300 microns wide. There was no significant changes in the oriens or pyramidale region (cell bodies) although extra cellular recording showed neural activity. They produced further evidence suggesting that the site of the activity induced changes in transmission was related to glial swelling due to the release of K⁺ during neuronal activity. Andrew and MacVicar found evidence that the transmission changes could not be attributed to glial swelling alone and ascribe the transmission changes to "swelling in dendrites and their adjacent glia". The

interaction between glia neurons and capillaries is well known. The application of glutamate causes swelling in cortical astroglia (Blankenfeld, Enkvist et al. 1995) and glia have been shown to be involved in a glutamate uptake in a glycolysis pathway coupling neural activity and glucose utilisation (Pellerin and Magistretti 1994 ; Kimelberg 1995).

There is thus evidence that the different signal sources may overlap considerably in terms of their spatial location (the neuropil). We suggest below that there is further 'overlap' in the interaction between the blood related and the tissue scattering sources.

The basic expression for absorption (the Beer-Lambert law) is :

$$A(\lambda) = \log \frac{I_0}{I(\lambda)} = \epsilon(\lambda).c.l$$

The parameters c and l refer to concentration and path length respectively and thus the product is the volume of the absorbing medium. The expression says that the absorption is proportional to the ratio of the incident and the measured illumination equals the product of the spectral coefficient and the volume of the sample. This expression will form the basis of the model we develop below, at this time however we wish to make the following point. In reflectance imaging it is not possible to distinguish between an increase in path length and an increase in blood volume (Jezzard, Heineman et al. 1994). The importance of this in the context of intrinsic imagery is that one of the primary signal sources increases the transmission characteristics of the underlying tissue and must thereby increase the path length and hence increase the volume of the 'visible' blood in the underlying tissue. Thus we use a simple mixture of transmission and reflectance model as the basis of the simulation. We assume that the increase in transmission decreases backscatter and though in a transmission model would be expected to increase the signal, in a reflectance model, can be treated as an increase in absorption. We make the further assumption that transmission increase in path length also effectively increases the volume and hence the absorption by the hemoglobin chromophores; and these two transmission related effects are additive. In summary, we make the assumption that the effect of neural activity on tissue transmission is twofold:

1. It decreases backscatter from neural tissue, causing a darkening of the image.
2. It interacts with the blood related signals by modulating the path length. This may well act to increase the spatial resolution by effectively amplifying differences from the more spatially diffuse blood volume and flow signals in regions of high neural activity.

We have evaluated the model (described below) under various conditions in which these two assumptions and the spatial resolution of the activity induced volume changes were manipulated. As one might expect, even with the volume resolution completely reduced spatial maps could be obtained under isobestic wavelength illumination. That is, when the only blood volume changes were those indirectly introduced by the modulation of path length by changes in the transmission signal source.

2.3 Spatial Modelling

Our model of the dynamics and spatial structure of the intrinsic signal sources contains the following further simplifying assumptions:

1. The complex neuronal-glia-capillary substrate can be modelled at each spatial position as a point source emitter of temporal signals directly affecting blood flow and volume, rate of deoxygenation, and a factor scaling the tissue transmission characteristics.
2. Under resting condition these signals are constant at unity. Following stimulation, they change according to the characteristics of their individual temporal response functions.
3. The amplitudes of the individual temporal responses are scaled proportionally to the stimulus preference function, though the value of the scale factor depends on the particular signal source and its spatial resolution.
4. The V-signal modulates both flow and volume, and its parameters vary both spatially and temporally, and are independent of the spatial preference function for neural activity.

Thus we identify four primary signals; they are: rate of blood flow, blood volume, rate of conversion of oxy-hemoglobin to deoxy-hemoglobin, and the transmission characteristics of the tissue. These signal outputs are nonlinearly combined to produce at each position an individual (image pixel) time series. The mechanisms that regulate blood flow and volume in response to increase in neural activity are not fully understood (for a review: (Villringer and Dirnagl 1995)) but there is evidence that they have a lower spatial resolution than the scattering and oxygen uptake signal sources. In our model these differences in the spatial resolution of the sources is embodied in the different values that are used to scale the stimulus preference function under the different stimulus conditions. A simple method for estimating the differential effects of the preferred and orthogonal stimuli on the different signal sources is to scale the stimulus preference function to the correct amplitude, and then convolve it with a unit volume gaussian function with sigma appropriate for the spatial resolution of particular signal source.

An approximation to the upper limit on the spatial resolution of the different signal sources is given by (Orbach and Cohen 1983). In an *in vitro* study, they estimated the degree of blurring of a small light source by brain tissue to be about 300 microns in diameter. The effect of this degree of blur in the context of an experimental mapping of the ocular dominance columns is quite marked, and even if the site of the signal sources was the sharply delineated input layer of the ocular dominance columns (IVc) the blur produced by the 300-500 microns of intervening tissue would be expected to remove any high frequency edge information from the intrinsic signal data. We make the assumption that all the signal sources are at the same depth of tissue and the estimates of their spatial resolution will include this component.

Thus to simulate a typical mapping experiment characteristic of the use of intrinsic imagery we model a region of cortex as a one-dimensional array (slice) of point sources to represent the activity of 'neurons' whose sensitivity to the stimulus dimension varies sinusoidally as a function of position along the array. One could imagine a slice cutting

across four ocular dominance column stripes and at each position the sensitivity to the left eye input is modelled as

$$P_L(n) = 0.5 \left(1 + \sin \left(2\pi \frac{n}{D} + \phi \right) \right)$$

and similarly, sensitivity to input from the right eye is 180 degrees out of phase:

$$P_R(n) = 0.5 \left(1 + \sin \left(2\pi \frac{n}{D} + \pi + \phi \right) \right)$$

Half the spatial period D can be regarded as the distance between the centres of adjacent ocular dominance columns (typically 500 microns Blasdel (1992)). Alternatively the preference profile could represent sensitivity to orientation, and manipulation of the phase component ϕ could be used to simulate the presentation of stimuli along a linear electrode track through different orientation columns. In these experiments we confine our analysis to an ocular dominance model. As described above, for each primary signal source there is a corresponding sensitivity function scaled and blurred to produce the values for the activity induced changes under the preferred and orthogonal stimulus conditions. Due to the low resolution of the signal sources (which are all lower than the tissue transmission blur) the sinusoidal stimulus preference function is relatively insensitive to errors in the estimates of the parameters of the scaling sensitivity and spatial resolution of the signal sources as they cannot change the shape of the sensitivity function. This ensures a fairer test of the analysis methodology.

2.4 Temporal modelling

Thus increased neural activity in so far as it results in: i) an increase in transmission, or ii) an increase in volume (either directly or indirectly), or iii) an increase in oxygen uptake will act to decrease the image intensity. Activity induced increase in flow, however, to the extent to which it 'flushes' out deoxygenated hemoglobin and replace it with new oxygenated blood will act to increase the image intensity. The image intensity is modelled by

$$I = I_0 \exp \left\{ -\gamma \left(A + B(C^o + C^r)(1+V) \right) \right\}$$

which is a lumped parameter expression relating the measured image intensity to the above signal sources. The parameters A , B , C^o , C^r and V are functions of both space n and time t in general, and are defined as follows.

Absorbance due to light scattering by brain tissue:

$$A = T(\lambda)(1 + \alpha(t, n))$$

$T(\lambda)$: The transmission spectrum scaling factor.

$\alpha(t, n)$: The neurally activated transmission temporal response function.

Absorbance due to interaction of scattering and blood volume effects:

$$B = \xi(t, \lambda)(1 + \beta(t, n))$$

$\xi(t, \lambda) = L(\lambda)(1 + \alpha(t, n))$: The path length volume transmission spectrum scaling factor.

Note that this scaling factor is affected by change in transmission characteristics.

$\beta(t, n)$: The neurally activated temporal response function; capillary recruitment say.

Modulation of the local blood volume by vasomotion:

$$(1 + V(t, n))$$

where V is a narrowband signal in time with frequency centred around 0.1Hz. It is also a function of space.

Hemoglobin concentration absorption:

$$C^o = H_o(\lambda) \left(S - \frac{\chi(1 + \rho(t, n))}{\mu(1 + \phi(t, n) + v(t, n))B'(1 + V(t, n))} \right)$$

In which:

$H_o(\lambda)$ is the spectrum for oxygenated hemoglobin. The parameter S is arterial saturation.

$\chi(1 + \rho(t, n))$: χ is the baseline oxygen reduction rate, and $\rho(t, n)$ is the function relating oxygen reduction to neural activity.

$\mu(1 + \phi(t, n) + v(t, n))$: the modulation of the baseline flow rate μ by neural activity ($\phi(t, n)$) and by vasomotion ($v(t, n)$).

$B' = (1 + \alpha(t, n))(1 + \beta(t, n))$: the transmission path length effect on overall volume.

The expression for the absorption due to the concentration of reduced hemoglobin is complementary and scaled by the absorbance spectrum for reduced hemoglobin.

$$C^r = H_r(\lambda) \left(1 - S + \frac{\chi(1 + \rho(t, n))}{\mu(1 + \phi(t, n) + v(t, n))B'(1 + V(t, n))} \right)$$

It is uncertain how the vasomotion signal is affected by neural activity (Golanov and Reis 1995; Mayhew, Askew et al. 1995; Morita, Hardebo et al. 1995) but for the purposes for simulation experiments we have regarded it as being independent of the stimulus conditions.

The model contains several functions relating (both directly and indirectly) neural activity to changes in parameter values. This involves assumptions concerning the dynamics of: i) the neural response to a stimulus presentation and ii) the transfer functions between neural

activity and the changes in blood flow rate etc. This is a dangerously uncharted area in which it is obviously difficult to be precise. The evidence from the literature is that the temporal response of the image data are very slow having time constants characteristically of the order of seconds (Frostig et al 1991, Malonek and Grinvald, 1995). It seems that changes in blood volume and flow are most delayed, occurring with post stimulus delays of two to three seconds and reaching their peak after about 5 seconds. In vitro studies of scattering suggest that this effect starts soon after the onset of stimulation and reaches its maximum in about three seconds. To the extent that scattering effects change the path length they will be confounded with blood volume related effects in the image data. The increase in the rate of oxygen uptake plausibly occurs almost immediately following stimulation, its time course is difficult to assess given the confounding with the increase in flow rate which occurs (Turner and Grinvald 1994). We have explored several ways to model the neural-signal source response functions in the study to be reported we use differently parameterised gamma functions.

2.5 Model Parameter Values

2.5.1 Caveats

The values of the model parameters were estimated from data reported in the neuroimaging and microcirculation literature and crudely hand crafted to match the largely qualitative descriptions of the temporal structure of the hemodynamics underlying intrinsic image data. Estimates of the spatial resolution of the different sources are particularly uncertain, and furthermore the values for the spatial and temporal parameters for the scattering and transmission signal source are largely derived from intrinsic signal data from *in vitro* preparations. The published estimates of the resolution from the intrinsic imaging data provided general constraints on the overall signal magnitudes. We tuned the model (with the V-signal omitted) into correspondence with the data from Frostig et al (1991). The model undoubtedly contains errors and inconsistencies arising from intra species differences (there is evidence of similarities between rats and humans (Blin, Ray et al. 1991)), the use of data from different brain regions and different preparations, and possibly even, errors of interpretation, but nevertheless it gives a plausible fit to some aspects of the published data.

2.5.2 Blood flow and volume parameters.

Fox et al(1986) report a 50% increase in flow rate following stimulation and a commensurate increase in glucose metabolism. Gjedde (1993) suggested the blood flow increase of ~25%, Kwong et al (1992) used estimates of 70% increase in flow. In our physiological data we find that the time course of the intrinsic signal (under 660 nm illumination) following stimulation typically shows a pronounced rebound effect. First the image darkens then it lightens for several seconds. We ascribe this to a delayed increase in flow replacing the deoxygenated blood and hence increasing saturation. Similar time series can be found in Grinvald et al (1986). On the other hand, Turner and Grinvald (1994) describe data "suggesting that capillaries in active tissue do not become hyperoxygenated", and that hyperoxygenation was only apparent in the venules (i.e., there is no contrast reversal or overshoot in parenchyma). We have evidence to the contrary

(Mayhew et al 1995), albeit in rat cortex and different stimulation. Meanwhile in our simulations we find that V-signal can mask the overshoot even at low amplitudes but manipulation of flow rate parameter could be used to produce either condition. With low increases in flow rate (~25%) the results described by Turner and Grindvald can be obtained; higher stimulus induced increases in flow rate (~70%) produces 'spectacular' overshoots. Of course there is some interaction with volume changes. Flow rates in different brain areas are known to vary several-fold (Nakagawa, Kin et al. 1995). In our experiments we scaled the increase in flow rate to give a small overshoot using a 50% increase in flow. The mapping signal should be relatively insensitive to the value of this parameter because the data is generally collected before the effects of the changes in flow manifest themselves. The temporal response function is modelled as a gamma function with mean and standard deviation of 4.5 and 1.5 sec respectively. This gives a temporal response delayed onset of about two seconds reaching a maximum at about 5 seconds (see Figure 1). To estimate the spatial resolution: Garthwaite and Boulton (1995) discuss the possibility that neuronal release of nitric oxide (a potent vasodilator) is one of the influences on local blood supply. Their estimation of the point spread diffusion of NO is about a 300 micron diameter sphere. (Paulson and Newman 1987) suggest the separation of arterioles maybe 500 microns or more and propose a glial potassium siphon as a mechanism for linking neural activity to increases in cerebral blood flow over these distances. It is known that glia have receptors for, and also release NO, thus the coupling between glia neuron and microvasculature may involve a serial pathway as well as a 'direct' diffusion path; this could act to reduce the spatial resolution. On the other hand, Lou (1987) proposes a highly local neural mechanism for the coupling with a resolution of 375 microns. We used the value of <500 microns radius (Greenberg, Hand et al. 1979) (cited Villinger and Dirnagl, 1995) from which to estimate the percentage increase under the orthogonal stimulus condition. This estimate for the spatial resolution is roughly equivalent to a gaussian blur with sigma 422 microns, giving an increase of 48% in blood flow under the orthogonal stimulus. This is rather coarser than might be suggested by the some of the studies above but seems more in accord with the resolution suggested by the intrinsic imaging literature. We model the blood volume parameters with the same temporal response functions as were used to model flow, but with slightly different spatial resolution. Fox et al (1986) report a ~15% increase in volume, (Belliveau, Kennedy et al. 1991) suggest about 30%; we use 20% and 19.5% for the preferred and orthogonal conditions which corresponds to a spatial resolution of ~480 microns.

2.5.3 Blood oxygenation parameters.

The baseline level of arterial saturation is generally greater than 90%. However as oxygen is lost increasingly as the surface to volume ratio increases, by the time it reaches the arterioles feeding the capillary beds, oxygen loss may be as high as 30% (Orrison et al 1995). We therefore assume the saturation of the new blood (the parameter S) in the model to be 70% and the baseline level of venous and capillary deoxygenation to be 50%. A parameter about which there is considerable controversy is the percentage increase in the consumption of oxygen induced by neural activity. The now classic paper by Fox et al (1986), using human subjects, found a 5% increase in oxygen consumption in contrast to the 51% increase in glucose consumption and 50% increase to rCBF. We find the mapping

signal very sensitive to variation in this parameter. If we constrain both the magnitude of the activity signal and the percentage mapping signal (at 630nm) to be of the same order as Frostig et al (1990), namely about 0.2% and 30-35% respectively; then we arrive at estimates of the percentage increases in oxygen uptake to be 9.5% and 8% under the preferred and orthogonal stimulus conditions; corresponding to a blur function with a sigma of 351 microns. A slight increase in the spatial resolution of the deoxygenation signal greatly increases the percentage mapping signal. The increase in oxygen uptake is known to be rapid (< 300 ms, Turner and Grinvald, 1994), (200-400ms, Frostig et al 1990). This function is modelled using a gamma function with mean and standard deviation of 2.5 and 1.0 sec respectively.

2.5.4 Tissue transmission parameters.

In *in vitro* studies of hippocampus, MacVicar and Hoffman (1991) found that an increase in transmission could be detected 2 seconds after stimulation onset. Holthoff et al 1994, reported the response to stimulation as "rather slow, reaching its maximum 3 seconds after onset of stimulation". We model the temporal characteristic with a gamma function with mean and standard deviation 3.5 and 1.0 sec respectively. To determine the values of the percentage change in transmission under the preferred and orthogonal stimulus conditions we adjusted them so that the activity signals and percentage mapping signals obtained under green (570nm) wavelengths were in the range reported by Frostig et al (1990). The values of the percentage change in transmission were set at 2.8% and 2.5% under the different stimulus conditions. This represents a spatial blur with a sigma of 375 microns, which is slightly less than the spatial resolution of the increase in oxygen uptake. We assume the path length parameters to be 0.5 and 0.2 under the red (630nm) and green (570nm) wavelengths. This is a rough estimate from LDF technical brochure and is dependent on the volume of blood in the tissue, we know of no other source for this parameter. We set the tissue absorption parameters under these two wavelengths to 0.6 and 6.0 respectively. For both these parameters it is their ratio that is important rather than absolute values. Wray et al (1988) report that scattering changes are wavelength independent at near IR wavelengths, and the studies by MacVicar and Hoffman (1991) and by Kreisman et al (1995) show similar spectral transmission functions in that the ratio $\Delta T/T$ increases from about 0.5 at 550nm upto about 0.8 at 630 to 650nm after which it is flat.

2.5.5 V-signal parameters.

The mechanism of the V-signal is uncertain. There is much evidence (the 1994, Perimed Reference List(12) contains a thousand or more references) that low frequency (~0.1Hz) oscillations can be found in the capillary beds in both peripheral (e.g. Schmidt et al 1995) and cerebral microcirculation (Morita et al 1995). Similar oscillations are also found *in vitro* studies of arterial vasomotion, e.g., (Osol and Halpern 1988; Griffith and Edwards 1994). Griffith and Edwards (1994) found that the oscillations may have chaotic patterns of behaviour. There are studies in brain which suggest that vasodilation and low frequency oscillations are neurogenic and can be triggered by stimulation from medulla and cerebellum. For example, Golanov et al (1994), Golanov and Reis (1995) distinguish spontaneous cerebrovascular waves (SCWs) which are saw-toothed in shape from other

spontaneous sinusoidal oscillations of rCBF. On the other hand, Morita et al (1995) found the amplitude and frequency of spontaneous cerebral vasomotion to be insensitive to section of sympathetic, parasympathetic and sensory nerves and they suggest a myogenic basis for vasomotion.

In our physiological data, we have found 'sinusoidal', complex (we hesitate to say chaotic, but they do have $1/f$ type spectra), and triangular shaped waveforms. For the purposes of evaluating the intrinsic imaging methodology the form of the oscillation may be quite important but to simplify we represent the V-signal in the simulations as a low frequency sinusoidal oscillation of 0.07Hz with constant amplitude. The amplitude of the signal is varied in different runs of the simulation between 0.5 and 1.5 % of the mean grey level. This maybe a conservative estimate of the V-signal amplitude (we have 67 minutes of recording of V-signal from cat hippocampus which has a mean amplitude of 3% of the mean grey level). The phase of the V-signal is varied smoothly as a function of position. The mathematical analysis (see Appendix A) uses a generic functional form for the V-signal.

2.5.6 Summary

The values of the parameters for the model are assumed to be spatially invariant as they are determined only by the neural sensitivity or preference function. However the phase and frequency of the V-signal under some conditions is assumed to vary smoothly as a function of position independently of the preference function. Systemic noise can be modelled with spatially correlated noise of the appropriate spectral content and power and spatially uncorrelated gaussian random noise source could be added to simulate image capture and camera noise. We excluded these noise sources from the experiments to simplify the evaluation. Figure 2 shows a time series from the simulation and from two experiments under red illumination for comparison. The time series have been normalised. The points to note are the relative magnitudes of the V-signal, they are very similar. However, the temporal response of the real data is significantly slower than in the simulation and lasts much longer than 10 secs (the usual period of data collection cycle). We have deliberately constrained the effects of stimulation to be complete before the onset of the next trial. Notwithstanding the time series generated by the simulation appears comparable to the real data sequences and also to the sequences shown in Grinvald et al (1986, 1991). While it is certain that our model is neither correct in all its details nor is it as complex as the real system, we believe the time series it generates provide a fair test of the methods of analysis and thereby a reasonable predictive estimate of performance on real data sequences.

3. Simulation

In this section we briefly review the method referred to as 'optical imaging spectroscopy' developed by Malonek and Grinvald (1995) and we describe simulated experiments to evaluate the methods for the analysis of intrinsic image data commonly used in the intrinsic imaging community (and recently recommended in a book chapter explaining the methodology by Bonhoeffer and Grinvald (1996)).

The study has two aims:

- i) to evaluate the accuracy and reliability of the 'maps' obtained using the 'usual' methodology. We also evaluate briefly the so-called *first frame analysis* method. This method is ascribed to D. Shoham by Bonhoeffer and Grinvald (1996). To counteract the effects of vascular arefacts the first 'frame' immediately following the stimulus and preceding any response is subtracted from the subsequent data before applying the usual analysis. It is very similar in effect to the method used by Blasdel (1992)
- ii) to evaluate the reliability of estimates of the contributions of the various signal sources to the intrinsic signal, in particular the use of the percentage mapping signal as an indication of the spatial resolution of the analysis method.

3.1 Malonek and Grinvald's method (Optical Imaging Spectroscopy)

In an ocular dominance column intrinsic imaging preparation in cat Malonek and Grinvald (1995) collected a set of time series data simultaneously under different wavelengths of illumination. They imaged a 'slice' of cortex using a diffraction grating spectroscope which spread the thin slice of cortex across the wavelengths to produce an image, one axis of which corresponded to the position along the slice, and positions along the other axis of the image corresponded to the slice illuminated under different wavelengths. They used least squares to solve for the coefficients $\theta(t)$ in the following linear model under orthogonal and preferred conditions of stimulation.

$$I(t, \lambda) = \theta_o(t).H_o(\lambda) + \theta_r(t).H_r(\lambda) + \theta_s(t)$$

This expression states that the image intensity (as a function of time and wavelength of illumination) is the weighted sum of the spectra for oxygenated and deoxygenated hemoglobin, and a wavelength independent term which corresponds to the absorption effects of the neural scattering effects.

Using the approximation

$$I(t, \lambda) = I_o \exp(-x) \approx I_o(1 - x)$$

when x is small and ignoring the constant original illumination intensity we can see the similarity between the equation

$$I(t, \lambda) = I_0 \exp\{-(\theta_o(t).H_o(\lambda) + \theta_r(t).H_r(\lambda) + \theta_s(t))\}$$

and the compressed form of our model:

$$I = I_0 \exp\{-\gamma(A + B(C^o + C^r)(1+V))\}$$

The coefficients θ_o and θ_r correspond to the volumes of the oxygenated and deoxygenated blood and correspond to $B.C^o$ and $B.C^r$ respectively, θ_s corresponds to A , the transmission term. This is assumed to be both wavelength independent in Malonek and Grinvald's equation. Superficially, there appears little difference between the two models (a constant and an overall scaling term of little importance). There are however deeper differences. The transmission term in Malonek and Grinvald's model varies only as a function of time, and is independent of the terms involving variation in blood volume, and of course there is no vasomotion or V -signal term in their equation. The fundamental differences between the two models is that Malonek and Grinvald's model contains no underlying hypothetical variables nor assumptions of the dynamics of their interactions (e.g., our model has parameters for increases in flow and volume of arterial supply and parameters for the oxygen reduction rate under resting and active conditions, and from these are derived the volumes of oxy- and deoxygenated blood that are 'unknowns' in Malonek and Grinvald's model). Thus their model is a linear statistical model in which the effects of the three signal sources are additive. An almost identical analysis was used by Wray et al (1988), as the basis for the calculation of changes in oxygenation of hemoglobin and cytochrome aa_3 . It has the advantage of being a simple descriptive model and the only dubious assumption made is that the spectrum of the activity induced scattering or transmission effect is constant over the wavelengths used (Malonek and Grinvald's experiment was conducted over a range of wavelengths (500-640nm) where this is unlikely to be correct (Kreisman et al, 1995, MacVicar and Hochman 1991), though it must be said that they were from *in vitro* studies). Malonek and Grinvald use their model to determine the temporal characteristics of the volumes of the oxygenated and deoxygenated blood and the activity induced changes in transmission. Comparison of the time series obtained from left and right ocular dominance columns, which were identified using the usual methodology, allowed Malonek and Grinvald to derive the time series of the mapping signal for the individual signal components (that is the difference between the responses to the preferred and orthogonal stimuli) and estimate the spatial resolution of the signal sources as the ratio of the amplitude of the mapping signal to the amplitude of the activity signal under the preferred stimulus conditions. Figure 4 shows a theoretical relationship between percentage mapping signal and spatial resolution (see section 3.3).

The summary of the results by Bonhoeffer and Grinvald (1996) is as follows:

1. rHB (oxygen uptake) volume. This signal had the highest spatial resolution, a ~30% mapping signal (corresponding to a blur function with a sigma of ~250 microns), and a fast temporal response (~200 ms) increasing during the stimulus and declining slowly towards base line (15-20 seconds).

2. HBO₂, The time series showed a small reduction in the first second or so, followed by a slow climb to a ~5% mapping signal (~375 microns) after about 5 seconds. This volume increase has the lowest spatial resolution
3. Light scattering. This mapping signal of this source was ~10% (~340 microns), wavelength independent, with a fast response (~200ms), coupled to the stimulus time course, decaying to base line within 3-4 seconds of stimulus offset.

These parameters do not map directly to the parameters of our model, however, we can extract the relevant data from the simulation in order to make the comparisons. From our model defined in Section 2 above, it is easy to show that the rHB volume is given by

$$rHB = L(\lambda) \left((1 + \alpha(t, n))(1 + \beta(t, n))(1 + V(t, n))S - \frac{\chi(1 + \rho(t, n))}{\mu(1 + \phi(t, n) + v(t, n))} \right)$$

the HBO₂ volume is given by

$$HBO_2 = L(\lambda) \left((1 + \alpha(t, n))(1 + \beta(t, n))(1 + V(t, n))(1 - S) + \frac{\chi(1 + \rho(t, n))}{\mu(1 + \phi(t, n) + v(t, n))} \right)$$

and the light scattering effect is given by

$$A = T(\lambda)(1 + \alpha(t, n))$$

Note that in our model, the equations for the volumes of deoxygenated and oxygenated blood contain an expression for the light scattering effect. The volume of blood 'under' each pixel is a function of the path length and this is determined by the spectral transmission characteristics of the tissue. Thus measures of blood volume are confounded with the wavelength of the illumination. (E.g., under near infra red illumination the brain becomes nearly transparent, the path length becomes very long, and hence the imaged blood volume becomes very large). In the calculation of the percentage mapping signal ratio the transmission and path length terms $L(\lambda)$ and $T(\lambda)$ in the numerator and denominator cancel. However, in the Malonek and Grinvald analysis they will be confounded in the estimates of the coefficients $\Theta(t)$ of the time series.

Figure 3(a) shows the time series for percentage mapping signal for the above three signals from the simulation. We find both the percentage mapping signals and their time courses are very different from those described by Bonhoeffer and Grinvald (1996, Figure 5). Our model is grounded by replicating the data from Frostig et al (1990). They used the 'usual' methodology for their analysis and reported a 5% mapping signal under 570nm illumination and ~30% mapping signal under 630nm (very similar to the values reported above for the HBO₂, and rHB volumes by Malonek and Grinvald). We adjusted parameters in the model to produce these values. However, when we do so, we find that whereas Malonek and Grinvald obtained a 5% mapping signal for the HBO₂ blood volume, we obtain only 2%; and for the rHB volume source we find only 6% compared to

their values of ~30%. From Figure 4 we see that the sigma of the resolution blur functions for the rHb signal source are, for our simulation, ~375 microns and for their real data, ~250 microns. The parameter most directly related to this signal source is the resolution of the activity induced increase in oxygen uptake, which in our model is ~350 microns. Again differences in the percentage mapping signal grossly amplify the differences in the underlying mechanism, but the point remains that using physiologically plausible values for the model parameters and adjusting them to fit the data reported by Frostig et al (1990) we obtain predicted blood volume values that are markedly different from those reported by Malonek and Grinvald (1995). These discrepancies await further investigation.

When the V-signal is included in the simulation the time series of the oxygenated and deoxygenated blood volume changes are affected (see Figure 3(b)) but in the simulation, our estimates of the time series of the transmission changes are independent of the V-signal. In Malonek and Grinvald's study their *model of the data* does not allow for any the temporal variation of the image data produced by the V-signal and independent of the stimulation regime. Thus their use of linear least squares methods will incorporate any such variation, as best it can, amongst the coefficients of the three time series $\Theta(t)$ in a way that minimises the overall residual error. It is difficult to predict the exact effect the of this confounding.

3.2 The 'usual' optical imaging methodology: Bonhoeffer and Grinvald (1996)

We examine the procedure frequently used in intrinsic imaging studies. The experimental cycle consists of a short (typically 2-3 sec) stimulus presented every 10 seconds. The stimulus conditions are counter balanced, randomised and interspersed with the presentation of a N(ull) stimulus condition. E.g. a typical stimulus sequence in an mapping experiment investigating ocular dominance might be the following: L-R-N-R-L-N-L-R-N... etc.

A block of trials consists of 8 or 16 permutations of the left eye, right eye and null stimulus triplets. Typically frames of video data are collected during the first three seconds of the cycle (sometimes only during the second and third seconds). The mean of this data provides the measurement for the particular trial. With the licence of simulation (but also in our physiological experiments) we collect the data as a continuous sequence and then subject it to different off-line analysis. The strategy of collecting only a few seconds of data immediately following the stimulation has advantages in that it is possible to finesse the very considerable data storage overheads. It is also justified on the grounds that it avoids corrupting the data with the low resolution increases in blood flow and volume which are known to have a slow delayed response to stimulation.

3.3 Terminology

Following practice in the literature we use the terms *global signal* and *activity signal* to refer to the change in image intensity produced by a particular stimulus condition. The map produced is called a *single condition map*. The change in image intensity is obtained by subtracting a genuine *blank* image from the image obtained after stimulation (dividing the image by the blank has almost identical effects). The blank image can be obtained in

several ways. It can be an image obtained during an interval when no stimulus was presented, or it can be the average image of all the images obtained during the different stimulus conditions, in the latter case it is called a *cocktail blank*. The difference between use of the two blanks is that the use of the *cocktail blank* forces the condition maps to become complementary, whereas if one uses a genuine *blank* the maps are not so constrained. The term *mapping signal* and, it seems, the term *differential map* is used when the map is produced by subtracting or dividing the images obtained from the presentation of two orthogonal stimulus conditions. Bonhoeffer (1995) have argued that these procedures are equivalent. *Differential maps* are necessarily complementary. They contain complementary vascular artefacts. The arithmetic definitions of the terms we use below in the analysis of the simulated data are as follows:

The activity signal is the change in reflected light which under the preferred condition, is given by $(I_{null} - I_{pref})$. Similarly under orthogonal condition, the activity is given by $(I_{null} - I_{orth})$. The normalised activity is the fractional change in reflected light. Under the preferred condition, normalised activity is given by

$$\Delta A = \frac{I_{null} - I_{pref}}{I_{null}}$$

Similarly under orthogonal condition,

$$\Delta B = \frac{I_{null} - I_{orth}}{I_{null}}$$

The mapping signal is given by

$$\text{Mapping} = I_{orth} - I_{pref}$$

The percentage mapping signal = $\frac{\Delta A - \Delta B}{\Delta A}$. This is the fraction of the normalised activity

signal which is specific to stimulus condition A. It can therefore be used to estimate the resolution of the mapping signal. Figure 4 is a plot of spatial resolution as a function the percentage mapping signal. We assumed that the underlying preference function is sinusoidal, that normalised activity under condition A is unity, and activity under condition B can be modeled by smoothing the preference function with a unit area gaussian. Using the spatial separation between the positive and negative peak of the preference function (500 microns) as the scale, the standard deviation of the blur function that produces a particular value of the percentage mapping signal can be used to estimate the resolution of the method. Figure 4 shows that differences in percentage mapping signals may give a slightly distorted indication of the differences in spatial resolution. For example the typical values (Frostig, Lieke et al. 1990) for the percentage mapping signal under 600nm and 570nm illumination respectively are 35% and 5%. A 35% mapping signal has a spatial

resolution of ~225 microns, whereas a 5% mapping signal has a spatial resolution of ~375 microns. What at first sight appears to be a seven fold improvement represents somewhat less in the spatial domain. Given that the magnitude of the activity signal under red illumination is at least an order of magnitude less than that under green, the optimal choice of detection strategy under conditions of noise and the presence of the V-signal could be subtle.

3.4 Reservations and predictions

The periodic 10 second data sampling strategy has the effect of aliasing with the low frequency modulation of the image intensity produced by the V-signal. The frequency of the V-signal varies around 0.1Hz and thus has a very similar period to the commonly adopted 10 second data collection cycle. It is to be expected that the variance in the activity mapping data will largely be determined by the power of the V-signal. The usual systemic noise sources (heart beat and breathing) can be smoothed out of the signal during data collection using cameras with long frame integration times (300ms or greater is common place), but whatever the frame rate used, the 'usual' methodology averages data collected over two or more seconds following the presentation of the stimulus and must contain low frequency components of the V-signal. Even if stimulus presentation and data collection were to be synchronised with the V-signal, the variance of the mean data collected on a single trial will reflect the phase in the V-signal cycle over which the data was collected (*i.e. to the extent that the V-signal is sinusoidal the variance is modulated as the differential; smaller at the peaks and greatest at the zero crossings*). If the V-signal is spatially invariant then its effect over the mapping region would be the same and there should be little spatial distortion of *the activity signal* profile. On the other hand, if there was any spatial variation of the amplitude, phase or frequency of the V-signal then it would be reflected in the means and variances of the intrinsic image data.

A mathematical analysis of the model described in Section 2 generated the following equations predicting the spatial structure of the activity and the differential maps (the analysis is presented in Appendix I).

$$\text{Activity} = \bar{I}_{null}(n) - \bar{I}_{pref}(n) = I_0\gamma(K_{DC} + K_P P(n) + K_V \bar{V}(n) + K_{PV} \bar{V}(n)P(n))$$

$$\text{Mapping} = \bar{I}_{orth}(n) - \bar{I}_{pref}(n) = 2I_0\gamma(K_P P(n) + K_{PV} \bar{V}(n)P(n))$$

where K_{DC} , K_V , K_P and K_{PV} are constant coefficients. The predictions derived from the above equations are:

1. The impact of spatial variation in the V-signal parameters will be greater in the case of the activity signals due to the presence of the $\bar{V}(n)$ term (the expected value of this term in the limit, is assumed to be the same under the different stimulus conditions. If it isn't the mathematics is harder and the impact is greater). If there is no spatial variation in the V-signal phase then there should be no distortion of the spatial structure produced by the two methods of analysis. It is common place in the imaging

literature that activity signals produce less reliable maps, and the mapping signal methods are adopted precisely because of the higher reliability of the maps produced.

2. The estimates of the resolution of the 'signal sources' in terms of the percentage mapping signal are effected by the V-signal even if there is no spatial variation. If there is spatial variation, then the estimates vary spatially. These estimates are particularly sensitive to bias in the data collection procedure caused by the beating of the data sampling period with the period of the V-signal.
3. Under isobestic illumination the impact of the V-signal spatial variation on the recovered spatial structure is greater than under non-isobestic illumination.

3.5 Results

Demonstration 1.

Figure 5 (a,b,c,d) shows results from a single 3 trial sequence consisting of a Null, Left and Right eye stimulus presentation using illumination at 630nm. (a) is a pseudo colour map. The horizontal axis represents position and the vertical axis is the temporal dimension. Thus each column in the figure represents the time series of the variation in intensity from a single pixel 'imaging' a particular position along the ocular dominance column 'brain tissue' slice. (b) shows two superimposed time series for pixels representing different preferred ocular dominance neurons. (c) shows three superimposed slices from across the temporal activity pattern under the different stimulation conditions. The slices represent imaged activity in the 2nd and 3rd seconds of each trial. (d) shows the activity maps (Null-Left)/Null and (Null-Right)/Null using the data from (c). The percentage mapping signal at the centre of the left ocular dominance column with the absence of the V-signal is 34.8%. Under 570nm illumination (not shown) the percentage mapping signal was 5.2%.

Demonstration 2.

Figure 6(a,b,c,d) is similar to Figure 5 but includes the V-signal with an amplitude of 0.5% (peak to peak one grey level). The phase of the V-signal varied linearly by 90° across the ocular dominance slice. The impact of phase variation on the activity signals is very obvious. No systemic noise was included in the simulation. The percentage mapping signal at the centre of the left ocular dominance column is found to be 156.7% and 25.6% under red and green illumination (green not shown). This shows the impact of the V-signal on the estimate of the percentage mapping signal on a single trial and the need for data averaging to remove its effect.

Experiment 1. *Spatially homogeneous V-signal*

Figure 7(a,b,c,d) shows results of a simulated experiment using illumination at 630nm. No systemic noise was added and the V-signal (amplitude 0.5%) was present without any phase variation across the ocular dominance slice. The data consists of 64 of the randomised Left-Right-Null 3 trial sequences. (a) shows a pseudo colour map in which the rows are mean of the data from the 2nd and 3rd seconds of each trial for the left eye's stimulus, the column positions of the map represent position in the slice across the ocular dominance columns. This clearly shows the effect of the V-signal on the individual trial

data. No clear overall stripe pattern corresponding to the ocular dominance preferences is discernible. However, when the data is grouped into eight blocks of eight, three trial sequences and averaged to produce eight maps the ocular dominance pattern becomes apparent, as shown in (b). (c) shows 'maps' of the *activity signals* obtained using a null condition blank, e.g., (Null-Left)/Null. The maps show little effect produced by the V-signal. This is as expected from the equation above for the activity signal that if the V-signal has no variation across the ocular dominance slice, the activity signal reflects the ocular dominance preference function $P(n)$. (d) shows the *mapping signal* Right-Left. In the map the structure of the ocular dominance column are clearly visible. In this case the percentage mapping signal is 34.8%. This resolution is equivalent to a gaussian blur function with sigma of ~230 microns. The effect of this V-signal is almost negligible.

Experiment 2. V-signal phase variation

Figure 8(a,b,c,d) shows results of a simulated experiment similar to Experiment 1. The only difference is that the V-signal phase varied linearly by 90 degrees across the ocular dominance slice. Again (a) is a pseudo colour map similar to that shown in Figure 8(a). It shows the effect of the V-signal phase variation on the individual trial data. The overall stripe pattern corresponding to the ocular dominance preferences is barely discernible. (b) shows that when the data is grouped into eight blocks of eight, three trial sequences and averaged to produce eight maps the ocular dominance pattern becomes apparent. (c) shows 'maps' of the *activity signal* obtained using a null condition blank, e.g., (Null-Left)/Null. In this case, the maps show considerable variation and the distorting effects produced by the V-signal are clear. This distortion is caused by the phase variation in the V-signal across the ocular dominance slice, as predicted by the activity equation above. (d) shows maps of the *mapping signals* obtained using Right-Left. In these maps the structure of the ocular dominance 'column' are readily seen and the biasing effects of the V-signal is nearly eliminated from the maps. The percentage mapping signal of the data shown is 45.0%. In a series of 6 experimental runs the value of the percentage mapping signal ranged from 27.7% to 45.0%, corresponding to a range of estimates of spatial resolution of ~275 to ~200 microns.

Experiment 3. Increased amplitude V-signal

Figure 9(a,b,c,d) shows results of a simulated experiment similar to Experiment 2 but in which the amplitude of the V-signal is increased to 1%. (a) is a pseudo colour map similar to that shown in Figure 8(a). The effect of the phase variation in the V-signal is marked though when averaged the ocular dominance pattern becomes apparent, as shown in (b). (c) shows 'maps' of the *activity signal*, (Null-Left)/Null. (d) shows maps of the *mapping signals* (Right-Left). The percentage mapping signal of the data shown is 55.9% and the range in a series of six experimental runs was 18.6 % to 55.9% corresponding to a range of spatial resolution of ~290 to ~ 170 microns. At a V-signal amplitude of 1.5% the range becomes 12.0% to 62.7% corresponding to ~325 to about ~155 microns.

Experiment 4. Isobestic Illumination.

The above experiments used 630nm wavelength illumination. Figure 10 shows similar data from experiments using illumination at the isobestic wavelength 570nm corresponding to

same experimental conditions as Experiment 1 (Figure 8 above). In the absence of the V-signal the percentage mapping signal was 5.2% (~375 microns), but with a 0.5% amplitude and a 90 degree phase variation the ranges (six 64 trial experimental runs) were 3.4% to 9.0% (~400 to ~350 microns). If the V-signal is increased to 1% the range becomes 1.1% to 13.7% (>500 to ~300 microns).

Experiment 5. *First frame analysis*

The assumptions underlying the so-called first frame analysis is that the frame (typically 300-450ms from a slow scan camera) immediately following the onset of the stimulus presentation contains only low frequency noise which will not change much over the duration of the simulation and thus may be sensibly subtracted from the data. Thus the first frame analysis method (at the risk of possibly increasing the noise by differencing the data prior to smoothing) may produce, on any particular trial, an activity map from which the low frequency 'vascular artefacts' have been removed.

Figure 11 shows the results of applying the first frame analysis method to the data from the same experimental conditions as in Experiment 3. The first mean of the first second of data was subtracted from the mean of the second and third seconds of data. It is clear that large proportion of the spatial distortion produced by the V-signal have been removed from both the activity signals (c) and to a lesser extent from the mapping signal (d).

This method has much in common with the method of data capture used by Blasdel (1992). He uses a voltage sensitive dye (NK2367) to obtain the signals and thus strictly speaking could be regarded as using extrinsic signals rather than intrinsic signals although the time over which he collects data are similar to those reported by others using intrinsic imagery. Blasdel uses the following data collection methodology. Under the different stimulus conditions the null condition and a stimulus are presented following each other in rapid succession for about 1-3 seconds each. Then after a delay of 10 seconds or so the sequence is repeated using the other stimulus. The order of the trials are counterbalanced and randomised, but on each trial a 'null' is collected and subtracted from stimulus data. The differential images or mapping signals produced by subtracting the means of the data from orthogonal stimulus conditions generate the functional maps of cortical architecture.

The effectiveness of both methods lies in the fact that the procedure of collecting the 'null' condition data in closer temporal proximity to the stimulus presentation induced data requires fewer trials to estimate the effect of the V-signal under that particular stimulus condition. It would be really interesting to see the differential maps produced by subtracting this first frame/null condition data collected 'adjacent' to the different stimulus conditions from each other.

In the limit, since all the analyses are linear and involve only means and differencing, the mapping signal recovered from the 'usual' methodology should be identical to the maps recovered using the first frame analysis and Blasdel's method. However the advantages of these methods are that there may be considerable savings in the number of trials needed to

produce satisfactory maps with the "desired signal-to-noise ratio" and the use of the first frame analysis "often salvaged experiments that otherwise would have been useless due to their large blood vessel artefacts" (Bonhoeffer and Givald, 1996).

Summary

The results of these simulation experiments show that maps obtained using an analysis that exploits the orthogonal stimulus conditions can represent the underlying 'physiology', despite the presence of the V-signal with reasonable accuracy. On the other hand maps of *activity signals* which use only a blank obtained during a null stimulus condition show a measure of bias introduced by the spatial inhomogeneity in the V-signal which is only eliminated by averaging many trials or, as in Experiment 5, by the use of the *first frame analysis* method. These results are almost exactly as are predicted from reports in the literature.

We find the standard errors of the activity signal means are generally of the same order or greater than the scaling space constant of the structures they are measuring. The 'scaling space constant' as the relationship between the image intensities and the spatial scale of the structures being mapped. For example given that the separation of the peaks (in image pixels) between the left and right ocular dominance columns corresponds to D microns of cortex (500 microns say); then, if I is the peak to peak difference (in grey level intensity, whatever the units used) in the image of cortical map, then a standard error of S in grey levels of intensity is scaled by D/I to represent the 'uncertainty' in terms of microns. Using this metric the size of the errors obtained in our simulations are of the order of 250 microns. Individual pixel standard errors primarily reflect the amplitude of the V-signal which is generally 5 to 10 times greater than the component of the *activity signal* due to neural activity, thus a statistical test based on the results from any single pixel would not be statistically significant. Methods for assessing the statistical reliability of intrinsic image maps are currently being investigated.

4. Conclusions

Our analysis and simulations have shown:

- The presence of the V-signal only introduces serious distortion of the shape of the functional maps obtained if there is a phase difference across the imaged area. If there is no spatial variation in the phase of the V-signal the shape of the obtained maps reliably and accurately match the stimulus preference function.
- The actual values obtained for both the activity and mapping signals however are affected by the presence of the V-signal independently of any phase variation. This effect can be reduced by collecting data from more trials but we find the estimates of the percentage mapping signal, even when there is no spatial variation in the phase of the V-signal, are unreliable compared to estimates made when the V-signal is absent. As expected, the effects of the V-signal are scaled by its amplitude.

- Experiments under isobestic illumination (~570 nm) are more susceptible to the effects of the V-signal. This maybe because at the isobestic point the deoxygenation (rHB) signal source which has the highest resolution is not present in the intrinsic signal data.
- In optical imaging spectroscopy the mapping signals are obtained by subtracting time series obtained under the preferred and orthogonal stimulus conditions from regions previously identified using the usual methodology. The V-signal in our simulation has an effect on the time series of the blood volume parameters (Figure 3), and hence estimates of the percentage mapping signal for the blood volume sources can be very different from the theoretical values.
- The method of first frame analysis does seem to provide a measure of control for the effects of the V-signal especially in the case of the activity signals. This may be of particular importance in imaging studies in which there is no obvious orthogonal stimulus condition enabling differential maps to be produced (e.g., intrinsic imaging studies of the barrel cortex in rat).

In conclusion, though we use estimates of the values of blood flow, volume and oxygenation uptake from the functional neuroimaging and microcirculation literature to parameterise the model, when the simulation includes the V-signal, the values of the mapping signal from the simulation are rarely as reported in the intrinsic imaging literature nor are the estimates of the percentage mapping as predicted from the model. On the other hand, if we tune the parameter settings so that in the absence of the V-signal the percentage mapping signals are a good fit to the reported values (Frostig, Lieke et al. 1990), the addition of the V-signal disrupts the estimates unless large numbers of trials are used. Grinvald (1991), recognising the presence of 'vascular artefacts', describes the use of a *post hoc* selection procedure when 96 out of 1280 trials (7.5 percent of the data) were used to produce the functional maps, though Frostig (1990) apparently only needed 10-64 trials per condition for their study.

However, and maybe more importantly for the purpose for which intrinsic imaging is mainly used (functional mapping of cortical architecture), the positional errors in our simulated functional maps are relatively small. If our data is representative, and it were possible to test the maps we obtained with a micro electrode to record the underlying neural selectivity (as commonly reported in the imaging community), the probability of a false match is very slight indeed, particularly if the electrode is inserted near the middle of the columns. The reliability of the positions of the boundaries is a somewhat different matter, and it should be remembered that we have not included any systemic and imaging noise in the simulation.

Notwithstanding the caveats concerning the correctness of our model (section 2.5.1) an issue of concern is the generality of the conclusions of our study. About the presence of the 'vascular artefacts' there can be no doubt, however reservations might be raised as to the magnitude of the V-signal amplitude and its effect in data previously reported in the literature. There are possibilities that the state of anaesthesia and the anaesthetic used in a particular physiological studies may have effects on the cerebral microcirculation and in particular the V-signal amplitude and frequency. Jones (1995) report that "cycling"

amplitude was greater under α -chloralose and halothane than under penobarbital anaesthesia though it was present under all three. Paradoxically, since intrinsic imaging of functional architecture is based on signal sources which one assumes require a normally functioning microcirculation, a reliable V-signal trace of the appropriate amplitude may be a desirable adjunct to the usual systemic monitoring variables. It has been shown, using LDF in rat, that variations in the level of mean arterial blood pressure (Morita, Bouskela et al. 1992) systematically affects both the amplitude and frequency of the vasomotion signal and sudden changes in blood pressure can be used to trigger the onset of "cycling" (Jones, Williams et al. 1995). Golanov et al (Golanov, Yamamoto et al. 1994; Golanov and Reis 1995) propose local networks of intracortical vasodilator neurons excited by remote extra cortical areas. Thus the V-signal, when better understood may provide an important systemic control, as well as being a source of 'vascular artefacts' to be removed or ignored at any cost.

We cannot draw firm conclusions concerning the reliability or otherwise of functional maps that previously have been obtained using intrinsic imagery. However we can with some measure of confidence propose the following generalities:

- It is now established that it is highly likely that in any preparation, the V-signal will be present in intrinsic imaging data in both parenchyma and the surface microvasculature whether it is looked for or not.
- Any spatial variation in the phase and amplitude of the V-signal is likely to impact on the functional maps obtained and analysed using the differential methodology, and particularly so when the experimental design does not lend itself to the comparison of data from orthogonal stimulus pairings though this can be in some part compensated for by the use of the method of first frame analysis.
- The statistical reliability of the conclusions of an imaging study are related fairly directly to power (variance) in the V-signal present during the data collection.
- It seems sensible to suggest that intrinsic imaging functional mapping studies should report the amplitude of the V-signal from the area of brain being investigated. It is a variable with potentially important impact on the reliability of the data, and is easily monitored either by LDF or by continuous video imaging.

5. Acknowledgements

This study was supported by grants from Sheffield University Research Fund. The authors are grateful to the other members of Brain Imaging Research Group for their advice, support and the *real* physiological data shown in Figure 2.

6. References

- Andrew, R. D. and B. A. MacVicar (1994). "Imaging cell volume changes and neuronal excitation in the hippocampal slice." *Neuroscience* 63(2): 371-383.
- Belliveau, D., D. Kennedy, et al. (1991). "Functional mapping of human visual cortex by magnetic resonance imaging." *Science* 254: 716-719.

- Blankenfeld, G. v., K. Enkvist, et al. (1995). Gamma-aminobutyric acid and glutamate receptors. Neuroglia. H. Kettenmann and B. R. Ransom. New York Oxford, Oxford University Press: 335-345.
- Glia
- Blasdel, G. G. (1992). "Differential imaging of ocular dominance and orientation selectivity in monkey striate cortex." Journal of Neuroscience 12(8): 3115-3138.
- Blasdel, G. G. (1992). "Orientation selectivity, preference, and continuity in monkey striate cortex." Journal of Neuroscience 12(8): 3139-3161.
- Blasdel, G. G. and G. Salama (1986). "Voltage-sensitive dyes reveal a modular organization in monkey striate cortex." Nature 321: 579-585.
- Blin, J., C. A. Ray, et al. (1991). "Regional cerebral glucose metabolism compared in rodents and humans." Brain Research 568: 215-222.
- Bonhoeffer, T., D. Kim, et al. (1995). "Optical imaging of the layout of functional domains in area 17 and across the area 17/18 border in cat visual cortex." Europ. J. Neuroscience: (in press).
- Cohen, L. B. (1973). "Changes in neuron structure during action potential propagation and synaptic transmission." Physiol. Rev. 53: 373-418.
- Dirnagl, G., U. Lindauer, et al. (1993). "Role of nitric oxide in the coupling of cerebral blood flow to neuronal activation in rats." Neuroscience Letters 149: 43-46.
- Fox, P. T., M. E. Raicic, et al. (1986). "Nonoxidative glucose consumption during focal physiologic neural activity." Science 241: 462-464.
- Frostig, R. D., E. E. Lieke, et al. (1990). "Cortical functional architecture and local coupling between neuronal activity and the microcirculation revealed by in vivo high-resolution optical imaging of intrinsic signals." Proc. Natn. Acad. Sci. U.S.A. 87: 6082-6086.
- Garthwaite, J. and C. L. Boulton (1995). "Nitric oxide signalling in the central nervous system." Annu. Rev. Physiol 57: 683-706.
- Gay, C. T., S. K. Brannan, et al. (1995). Part I. Brain function mapping. Diffusion and Perfusion Magnetic Resonance Imaging. D. I. Bihan, Raven Press: 217-226.
- Gjedde, A. (1993). Interpretating physiology maps of the living human brain. Quantification of Brain Functions. K. Uemura. Amsterdam/New York, Elsevier Science Publishers: 187-196.
- Golanov, E. V. and D. Reis (1995). "Vasodilation evoked from medulla and cerebellum is coupled to bursts of cortical EEG activity in rats." J. Am. Physiol. 268 (Regulatory Integrative Comp. Physiol. 38): R454-R467.
- Golanov, E. V., S. Yamamoto, et al. (1994). "Spontaneous waves of cerebral blood flow associated with a pattern of electrocortical activity." J. Am. Physiol. 266 (Regulatory Integrative Comp. Physiol. 35): R204-R214.
- Golanov, E. V., S. Yamamoto, et al. (1994). "Spontaneous waves of cerebral blood flow associated with a pattern of electrocortical activity." Am. J. Physiol. 266: R204-214.

- Greenberg, J., P. Hand, et al. (1979). "Localised metabolic-flow couple during functional activity." Acta Neurol. Scand. 60(Suppl 72): 1230-1234.
- Griffith, T. M. and D. H. Edwards (1994). "EDRF suppresses chaotic oscillations in isolated resistance artery without influencing intrinsic complexity." Am. J. Physiol. 266 (Heart Circ. Physiol.): H1786-1800.
- Grinvald, A., R. D. Frostig, et al. (1988). "Optical imaging of neuronal activity." Physiol Rev. 68: 1285-1365.
- Grinvald, A., R. D. Frostig, et al. (1991). "High-resolution optical imaging of functional brain architecture in the awake monkey." Proc. Natl. Acad. Sci. USA 88: 11559-11563.
- Grinvald, A., E. Lieke, et al. (1986). "Functional architecture of cortex revealed by optical imaging of intrinsic signals." Nature 324: 361-364.
- Hill, D. K. and R. D. Keynes (1949). "Opacity changes in the stimulated nerve." J. Physiol. Lond. 108: 278-281.
- Iadecola, C. (1993). "Regulation of the cerebral microcirculation during neural activity: is nitric oxide the missing link?" Trends in Neuroscience 16(6): 206-214.
- Jezzard, P., F. Heineman, et al. (1994). "Comparison of EPI gradient-echo contrast changes in cat brain caused by respiratory challenges with direct simultaneous of cerebral oxygenation via a cranial window." NMR in Biomedicine 7: 35-44.
- Jones, S. K., J. L. Williams, et al. (1995). "Cortical cerebral blood flow cyclin: anesthesia and arterial blood pressure." A. J. Physiol. 268 (Heart Circ. Physiol. 37): H569-H575.
- Jueptner, M. and C. Weiller (1995). "Review: Does measurement of regional cerebral blood flow reflect synaptic activity? - Implications for PET and fMRI." Neuroimage 2: 148-156.
- Kimelberg, H. K. (1995). Brain Edema. Neuroglia. H. Kettenmann and B. R. Ransom. New York Oxford, Oxford University Press: 919-935.
- Lipton, P. (1973). "Effects of membrane depolarization on light scattering by cerebral cortical slices." J. Physiol. (Lond.) 231: 365-383.
- Lou, H., L. Edvinsson, et al. (1987). "The concept of coupling blood flow to brain function: a revision required?" Ann. Neurol 22: 289-297.
- MacVicar, B. A. and D. Hochman (1991). "Imaging of synaptically evoked intrinsic signals in hippocampal slices." J. Neurosci. 11: 1458-1469.
- Malonek, D. and A. Grinvald (1995). "The spatial and temporal relationship between cortical electrical activity and responses of the microcirculation during sensory stimulation." Soc. Neurosci. Abstr. 21: 311.11.
- Masino, S. A., M. C. Kwon, et al. (1993). "Characterisation of functional organisation within rat barrel cortex using intrinsic signal optical imaging through a thinned skull." Proc. Natl. Acad. Sci. USA 90: 9998-10002.
- Mayhew, J. E. W., S. Askew, et al. (1995). "Cerebral vasomotion: 0.1Hz oscillation in imaging of neural activity." Soc. Neurosci. Abstr. 21: 656.9.

- Mayhew, J. E. W., S. Askew, et al. (1996). "Cerebral vasomotion: 0.1Hz oscillation in imaging of neural activity." in preparation.
- Morita, Y., E. Bouskela, et al. (1992). "Vasomotion in the rat cerebral microcirculation recorded by laser-doppler flowmetry." Acta Physiol. Scand **146**: 431-439.
- Morita, Y., J. E. Hardebo, et al. (1995). "Influence of cerebrovascular sympathetic, parasympathetic, and sensory nerves on autoregulation and spontaneous vasomotion." Acta Physiol Scand **154**: 121-130.
- Nakagawa, H., S.-Z. Kin, et al. (1995). Blood volumes, hematocrits and transit times in parenchymal microvascular systems. Diffusion and Perfusion Magnetic Resonance Imaging. D. I. Bihan, Raven Press: 193-200.
- Orbach, H. S. and L. B. Cohen (1983). "Optical monitoring of activity from many areas of the in vitro and in vivo salamander olfactory bulb: A new method for studying functional organization in the vertebrate central nervous system." J. Neuroscience **3**: 2251-2262.
- Orrison, W. W., J. D. Lewine, et al. (1995). Functional Brain Imaging, Mosby.
- Orrison, W. W. and J. A. Sanders (1995). Functional Magnetic Imaging. Functional Brain Imaging. W. W. Orrison, J. D. Lewine, J. A. Sanders and M. F. Hartshorne, Mosby: 239-326.
- Osol, G. and W. Halpern (1988). "Spontaneous vasomotion in pressurized cerebral arteries from genetically hypertensive rats." Am. J. Physiol. **254** (Heart Circ, Physiol. **23**): H28-H33.
- Paulson, O. B. and E. A. Newman (1987). "Does the release of potassium from astrocyte endfeet regulate cerebral blood flow." Science **237**: 896-898.
- Pellerin, L. and P. J. Magistretti (1994). "Glutamate uptake into astrocytes stimulates aerobic glycolysis: a mechanism coupling neuronal activity to glucose utilisation." Proc. Natl. Acad. Sci. USA **91**: 10625-10629.
- Shepherd, A. P. and P. A. Oberg (1990). Laser Doppler Flowmetry. Norwell MA, USA, Kluwer Academic Publishers.
- Ts'o, D. Y., R. D. Frostig, et al. (1990). "Functional organization of primate visual cortex revealed by high resolution optical imaging." Science **249**: 417-420.
- Turner, R. and A. Grinvald (1994). "Direct visualisation of patterns of deoxygenation and reoxygenation in monkey cortical vasculature during functional brain activation." Proc. Soc. Magn. Res.: 430.
- Villringer, A. and U. Dirnagl (1995). "Coupling of brain activity and cerebral blood flow: Basis of functional neuroimaging." Cerebrovascular and Brain Mechanism Reviews **7**: 240-276.
- Wray, S., M. Cope, et al. (1988). "Characterisation of near infrared absorption spectra of cytochrome oxidase aa₃ and haemoglobin for the non invasive monitoring of cerebral oxidation." Biochimica et Biophysica Acta **933**: 184-192.
- Zee, P. V. d. and D. T. Delpy (1988). "Computed point spread functions for light in tissue using a measured volume scattering function." Adv. in Exp. Med. and Biol. **222**: 191-197.

Appendix A

The intensity equation used to model the intrinsic image intensity is

$$I = I_0 \exp\{-\gamma[A + B(C^o + C')](1 + V)\} \quad (A1)$$

where A , B , C^o , C' and V are functions of both space n and time t in general, and are defined as follows.

Absorbance due to light scattering by brain tissue :

$$A = T(\lambda)(1 + \alpha(t, n))$$

$T(\lambda)$: The transmission spectrum scaling factor.

$\alpha(t, n)$: The neurally activated temporal response function.

Absorbance due to interaction of scattering and blood volume effects:

$$B = \xi(t, \lambda)(1 + \beta(t, n))$$

$\xi(t, \lambda) = L(\lambda)(1 + \alpha(t, n))$: The path length volume transmission spectrum scaling factor.

Note that this scaling factor is affected by change in transmission characteristics.

$\beta(t, n)$: The neurally activated temporal response function; capillary recruitment say.

Modulation of the local blood volume by vasomotion:

$$(1 + V(t, n))$$

where V is a narrowband signal in time with frequency centred around 0.1Hz. It is also a function of space.

Hemoglobin concentration absorbtion.

$$C^o = H_o(\lambda) \left(S - \left(\frac{\chi(1 + \rho(t, n))}{\mu(1 + \phi(t, n) + \nu(t, n))} \cdot \frac{1}{B'(1 + V)} \right) \right)$$

In which:

$H_o(\lambda)$ is the oxygenated hemoglobin spectrum. The parameter S is arterial saturation.

$\chi(1 + \rho(t, n))$: χ is the baseline oxygen reduction rate, and $\rho(t, n)$ is the function relating the change in oxygen reduction due to increased neural activity.

$\mu(1 + \phi(t, n) + \nu(t, n))$: μ is the baseline blood flow rate; it is modulated by neural activity $\phi(t, n)$ and by vasomotion $\nu(t, n)$.

$B' = (1 + \alpha(t, n)) \cdot (1 + \beta(t, n))$: the transmission path length effect on overall volume.

The expression for the **absorption due to the concentration of reduced hemoglobin** is complementary and scaled by the absorbance spectrum for reduced hemoglobin.

$$C' = H_r(\lambda) \left(1 - S + \left(\frac{\chi(1 + \rho(t, n))}{\mu(1 + \phi(t, n) + v(t, n))} \cdot \frac{1}{B'(1 + V)} \right) \right)$$

From eqn.(A1), as the whole term in the power of the exponential is very small, it can be approximated by

$$I = I_0 \{ 1 - \gamma [A + B(C^o + C')(1 + V)] \}$$

Under the null condition, there is no stimuli present and assuming any effects of resting level neural 'noise' are negligible, the above model parameters can be simplified to the following :

$$A = T(\lambda), \quad B = L(\lambda),$$

$$C^o = H_o(\lambda) \left(S - \frac{\chi}{\mu(1 + v(t, n))} \cdot \frac{1}{(1 + V)} \right),$$

$$C' = H_r(\lambda) \left(1 - S + \frac{\chi}{\mu(1 + v(t, n))} \cdot \frac{1}{(1 + V)} \right)$$

The intensity signal under null condition can then be written as

$$I_{null} = I_0 \left\{ 1 - \gamma \left[T + L(1 + V(t, n))(H_o S + H_r(1 - S)) + L(H_r - H_o) \frac{\chi}{\mu(1 + v(t, n))} \right] \right\} \quad (A2)$$

Note that the wavelength λ has been omitted in the above equation to simplify the notation. The equation shows that under the null stimulus condition, the intensity of the image obtained is a nonlinear function of the V-signal. By assuming that the amplitude of the V-signal is much less than unity, the above equation can be written as

$$I_{null} = I_0 \{ 1 - \gamma [T + L(1 + V(t, n))H + J_{null}(t, n)] \}$$

where

$$H = H_o S + H_r(1 - S)$$

and

$$J_{null}(t, n) = L(H_r - H_o) \frac{\chi}{\mu} (1 - v(t, n))$$

Under stimulation conditions, the response functions α , β , ρ and ϕ are present and are also functions of space. If the stimulus preference functions of the ocular dominance

columns are represented by $P_{pref}(n)$ and $P_{orth}(n)$ which are smooth zero-mean functions of space, and making the usual physiological assumption that

$$P_{pref}(n) = -P_{orth}(n) = P(n)$$

then the response due to transmission change can be written as

$$\alpha(t, n) = \begin{cases} \frac{\alpha_a(t) - \alpha_b(t)}{2} P(n) + \frac{\alpha_a(t) + \alpha_b(t)}{2} = \alpha_{pref}, & \text{(preferred condition)} \\ \frac{\alpha_a(t) - \alpha_b(t)}{2} (-P(n)) + \frac{\alpha_a(t) + \alpha_b(t)}{2} = \alpha_{orth}, & \text{(orthogonal condition)} \end{cases} \quad (A3)$$

where $\alpha_a(t)$ is the temporal response function representing activity from neurons at the centre of an ocular dominance column when stimulated by the preferred stimulus, and $\alpha_b(t)$ is the temporal response function when stimulated by the orthogonal stimulus.

Similarly the response due to blood volume change can be written as

$$\beta(t, n) = \begin{cases} \frac{\beta_a(t) - \beta_b(t)}{2} P(n) + \frac{\beta_a(t) + \beta_b(t)}{2} = \beta_{pref}, & \text{(preferred condition)} \\ \frac{\beta_a(t) - \beta_b(t)}{2} (-P(n)) + \frac{\beta_a(t) + \beta_b(t)}{2} = \beta_{orth}, & \text{(orthogonal condition)} \end{cases} \quad (A4)$$

The response function due to change in oxygen reduction rate can be written as

$$\rho(t, n) = \begin{cases} \frac{\rho_a(t) - \rho_b(t)}{2} P(n) + \frac{\rho_a(t) + \rho_b(t)}{2} = \rho_{pref}, & \text{(preferred condition)} \\ \frac{\rho_a(t) - \rho_b(t)}{2} (-P(n)) + \frac{\rho_a(t) + \rho_b(t)}{2} = \rho_{orth}, & \text{(orthogonal condition)} \end{cases} \quad (A5)$$

and the response function due to blood flow rate change can be written as

$$\phi(t, n) = \begin{cases} \frac{\phi_a(t) - \phi_b(t)}{2} P(n) + \frac{\phi_a(t) + \phi_b(t)}{2} = \phi_{pref}, & \text{(preferred condition)} \\ \frac{\phi_a(t) - \phi_b(t)}{2} (-P(n)) + \frac{\phi_a(t) + \phi_b(t)}{2} = \phi_{orth}, & \text{(orthogonal condition)} \end{cases} \quad (A6)$$

Now under the preferred condition,

$$I_{pref} = I_o \left\{ 1 - \gamma \left[T(1 + \alpha_{pref}) + L(1 + \alpha_{pref})(1 + \beta_{pref})(1 + V(t, n))H + J_{pref}(t, n) \right] \right\}$$

where

$$J_{pref}(t, n) = L(H_r - H_o) \frac{\chi(1 + \rho_{pref})}{\mu(1 + \phi_{pref} + v(t, n))}$$

If one makes the assumption that during the data collection period, the change in flow is significantly less than unity, and that the amplitude of the V-signal, $v(t, n)$, is also much less than unity, then by ignoring higher order terms, I_{pref} and J_{pref} can be rewritten as

$$I_{pref} = I_o \left\{ 1 - \gamma \left[T(1 + \alpha_{pref}) + L(1 + \alpha_{pref} + \beta_{pref})(1 + V(t, n))H + J_{pref}(t, n) \right] \right\}$$

where

$$J_{pref}(t, n) = L(H_r - H_o) \frac{\chi}{\mu} (1 + \rho_{pref} - \phi_{pref} - v)$$

Similarly under the orthogonal condition,

$$I_{orth} = I_o \left\{ 1 - \gamma \left[T(1 + \alpha_{orth}) + L(1 + \alpha_{orth} + \beta_{orth})(1 + V(t, n))H + J_{orth}(t, n) \right] \right\}$$

where

$$J_{orth}(t, n) = L(H_r - H_o) \frac{\chi}{\mu} (1 + \rho_{orth} - \phi_{orth} - v)$$

Now let's consider the effect of sampling the intensity signal under various stimulation conditions. To avoid even more tedious algebra, we assume instantaneous sampling. It is also reasonable to assume that data is collected at a fixed time after the onset of each stimulus (including the null stimulus), therefore the parameters α_{pref} , α_{orth} , β_{pref} , β_{orth} etc are invariant with respect to sampling instants. Furthermore, we make the assumption

that if data is collected over a large number of trials, the mean values of the V-signal under different stimulus conditions will be sufficiently close such that

$$\bar{V}(t, n)|_{null} = \bar{V}(t, n)|_{pref} = \bar{V}(t, n)|_{orth} = \bar{V}(n)$$

and

$$\bar{v}(t, n)|_{null} = \bar{v}(t, n)|_{pref} = \bar{v}(t, n)|_{orth} = \bar{v}(n)$$

This will enable us to write the activity signal as follows.

$$\bar{I}_{null}(n) - \bar{I}_{pref}(n) = I_0 \gamma \left\{ T \alpha_{pref} + L(\alpha_{pref} + \beta_{pref})(1 + \bar{V}(n))H + (J_{pref} - J_{null}) \right\}$$

where

$$J_{pref} - J_{null} = L(H_r - H_o) \frac{\chi}{\mu} (\rho_{pref} - \phi_{pref})$$

Substituting equations (A3)-(A7) to the above and after simple manipulations and ignoring higher order terms, the activity signal can be written as

$$\text{Activity} = \bar{I}_{null}(n) - \bar{I}_{pref}(n) = I_0 \gamma (K_{DC} + K_P P(n) + K_V \bar{V}(n) + K_{PV} \bar{V}(n) P(n)) \quad (A7)$$

where

$$K_V = \frac{LH}{2} (\alpha_a + \alpha_b + \beta_a + \beta_b)$$

$$K_{DC} = \frac{T}{2} (\alpha_a + \alpha_b) + K_V + \frac{L(H_r - H_o)}{2} \frac{\chi}{\mu} (\rho_a + \rho_b - (\phi_a + \phi_b))$$

$$K_{PV} = \frac{LH}{2} (\alpha_a - \alpha_b + \beta_a - \beta_b)$$

$$K_P = \frac{T}{2} (\alpha_a - \alpha_b) + K_{PV} + \frac{L(H_r - H_o)}{2} \frac{\chi}{\mu} (\rho_a - \rho_b - (\phi_a - \phi_b))$$

On the other hand, the mapping signal is given by

$$\bar{I}_{orth}(n) - \bar{I}_{pref}(n) = I_0 \gamma \left\{ T(\alpha_{pref} - \alpha_{orth}) + L(\alpha_{pref} - \alpha_{orth} + \beta_{pref} - \beta_{orth})(1 + \bar{V}(n)) + (J_{pref} - J_{orth}) \right\}$$

where

$$J_{pref} - J_{orth} = L(H_r - H_o) \frac{\chi}{\mu} (\rho_{pref} - \rho_{orth} - (\phi_{pref} - \phi_{orth}))$$

Again after substituting equations (A3)-(A6) into the above, the mapping signal can be shown to be

$$\text{Mapping} = \bar{I}_{orth}(n) - \bar{I}_{pref}(n) = 2I_0 \gamma (K_p P(n) + K_{pV} \bar{V}(n) P(n)) \quad (\text{A8})$$

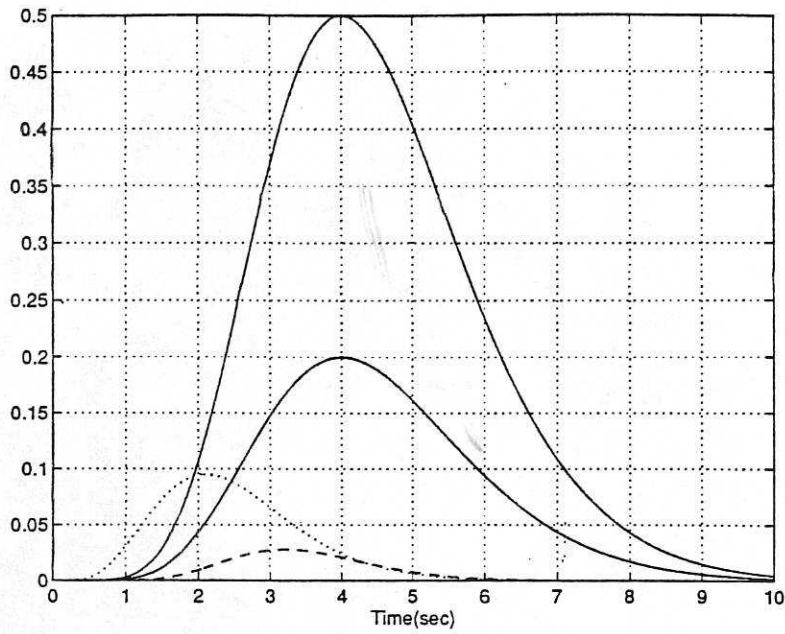


Figure 1. Temporal response functions of signal sources. *Solid line:* Increase in percentage flow rate. *Dash-dot line:* Increase in percentage blood volume. *Dotted line:* Increase in oxygen uptake. *Dashed line:* Increase in scattering induced transmission characteristics.

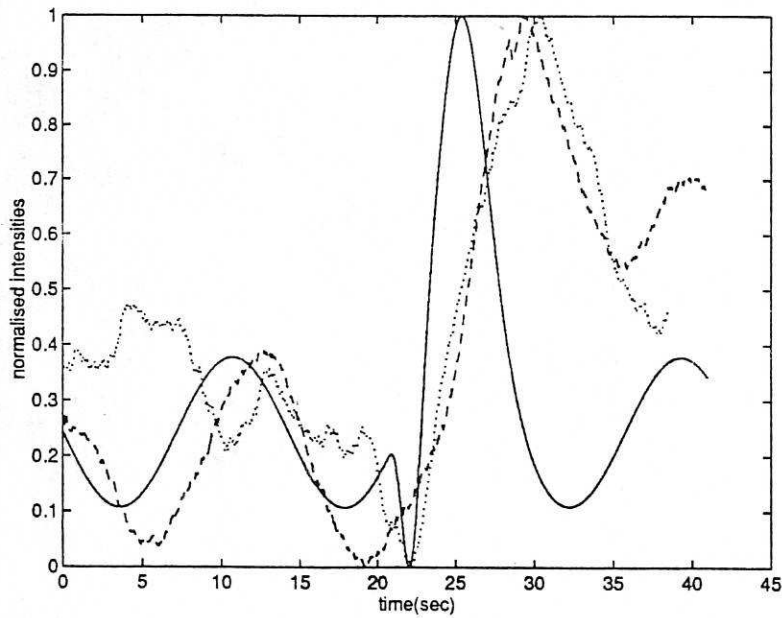


Figure 2. Comparison of real data and simulated data. *Solid line:* Simulation *Dashed line, dotted line:* Mean time series from stimulation of sensory motor cortex of rat. Two seconds nociceptive stimulation at 20 seconds.

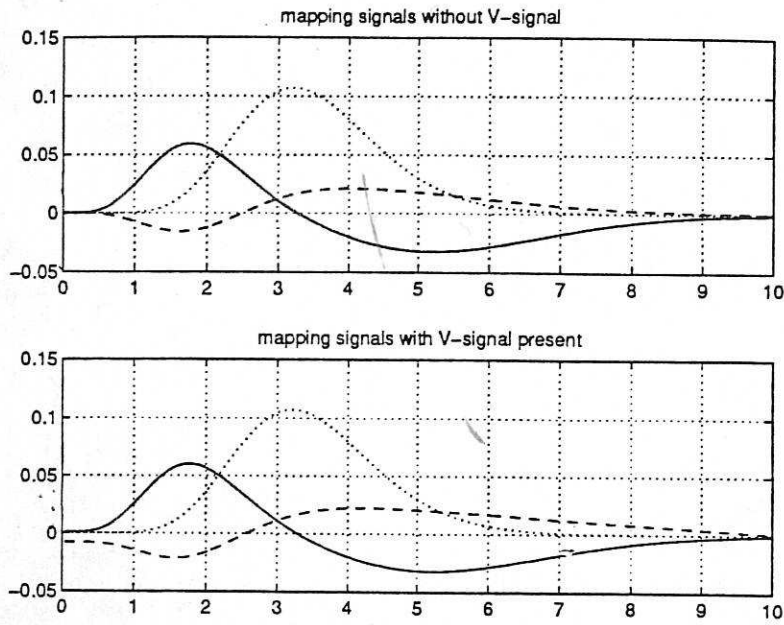


Figure 3 Percentage mapping signals using volumes of rHB, HBO₂ and tissue transmission signal sources. *Solid line: rHB. Dashed line: HBO₂, Dotted line: Transmission.*

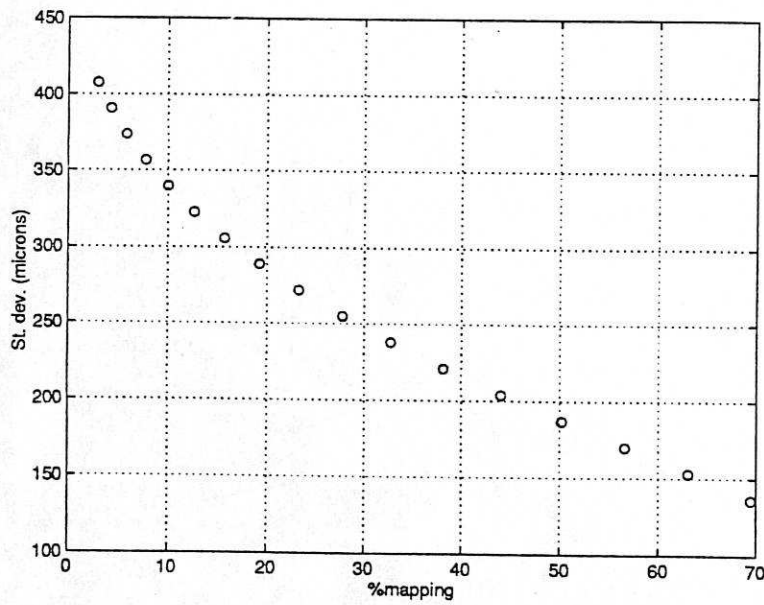


Figure 4. Relationship between the standard deviation of a gaussian 'blur' function and the percentage mapping signal as a measure of spatial resolution.

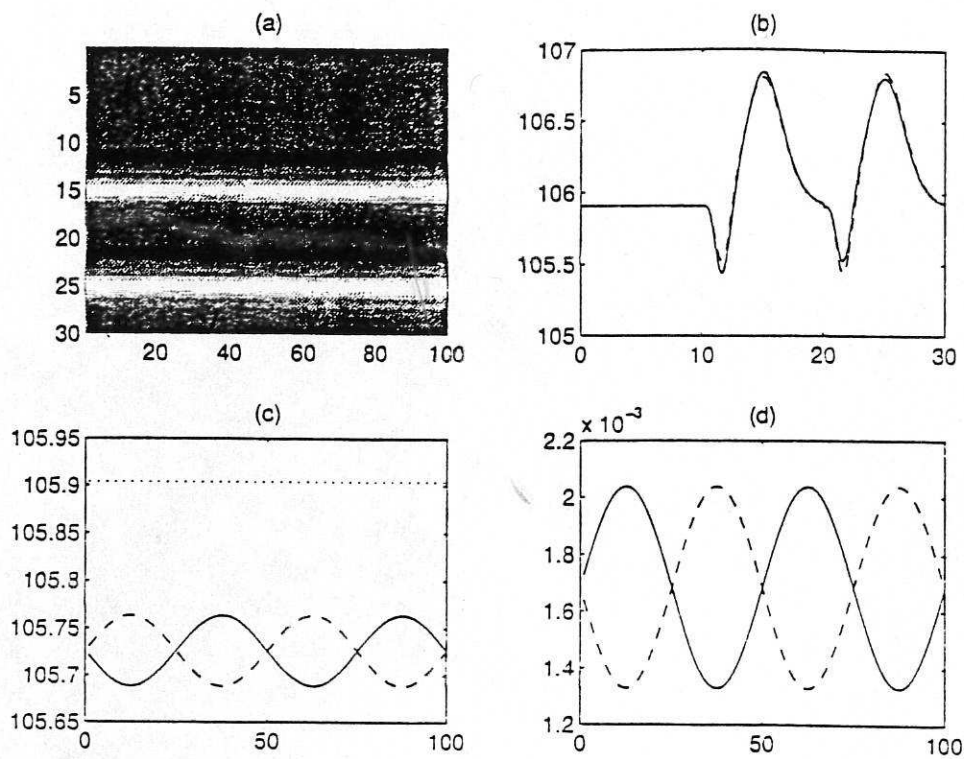


Figure 5. Demonstration 1. Data from a single 3 trial sequence without the V-signal.

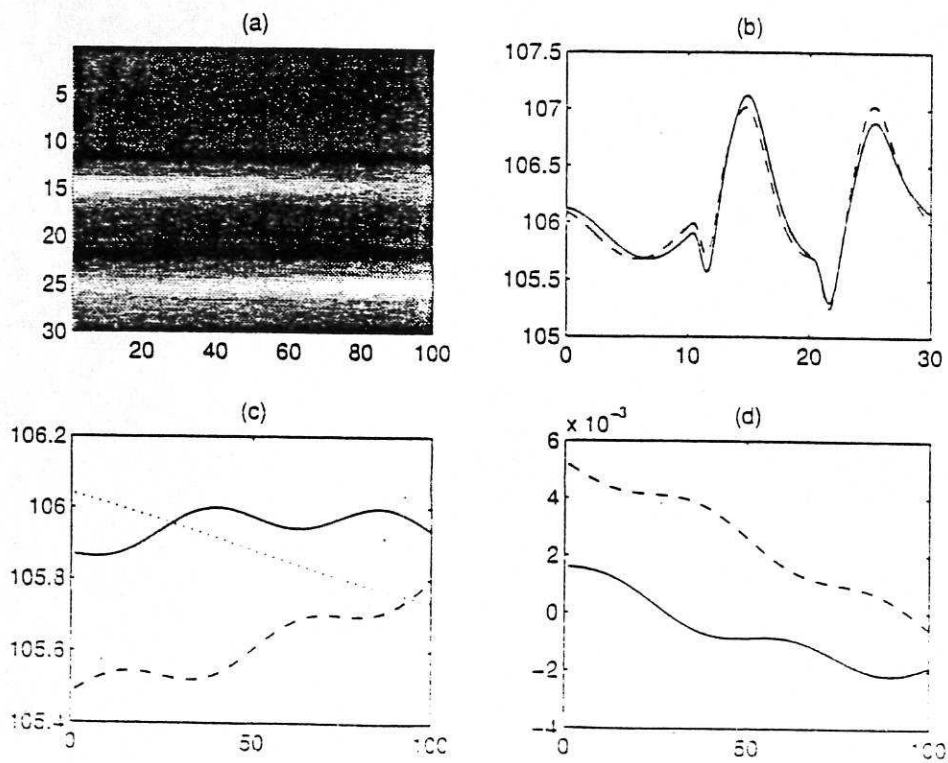


Figure 6. Demonstration 2. Data from a single 3 trial sequence with the V-signal.

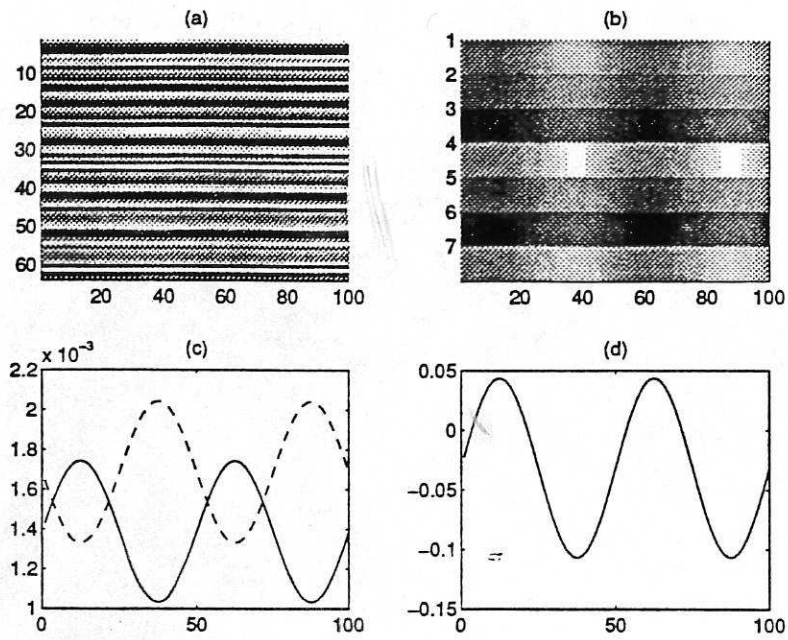


Figure 7. Experiment 1. Spatially homogeneous V-signal.

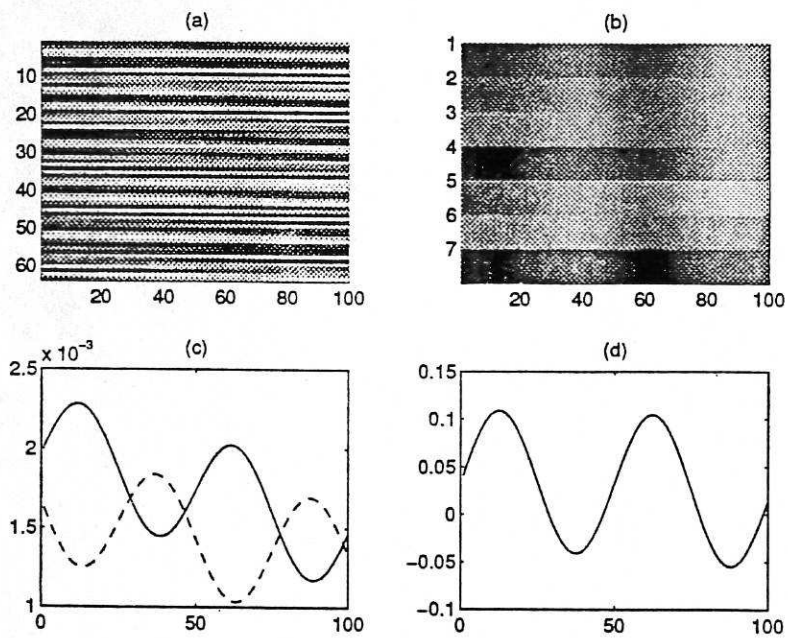


Figure 8. Experiment 2. V-signal 90° phase variation

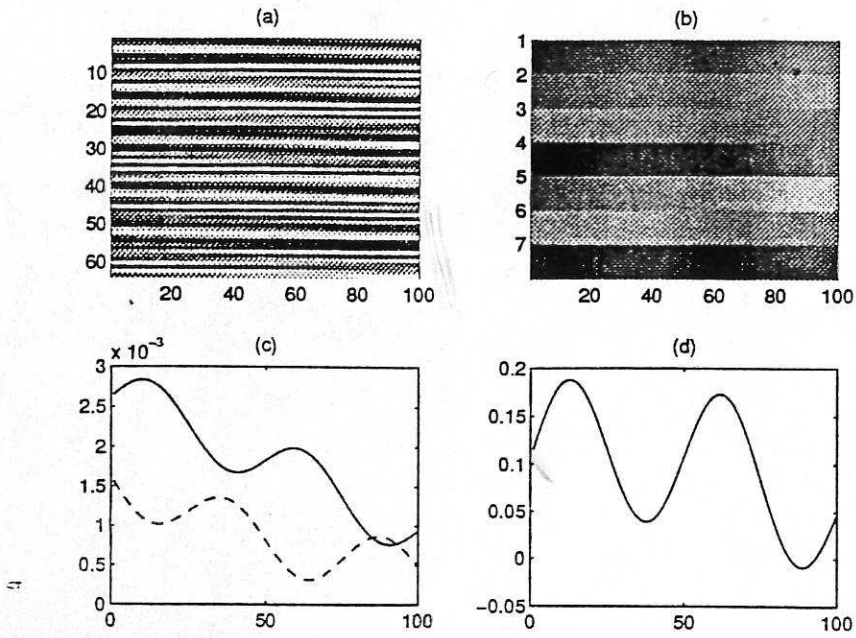


Figure 9. Experiment 3. Increased amplitude of V-signal (1%)

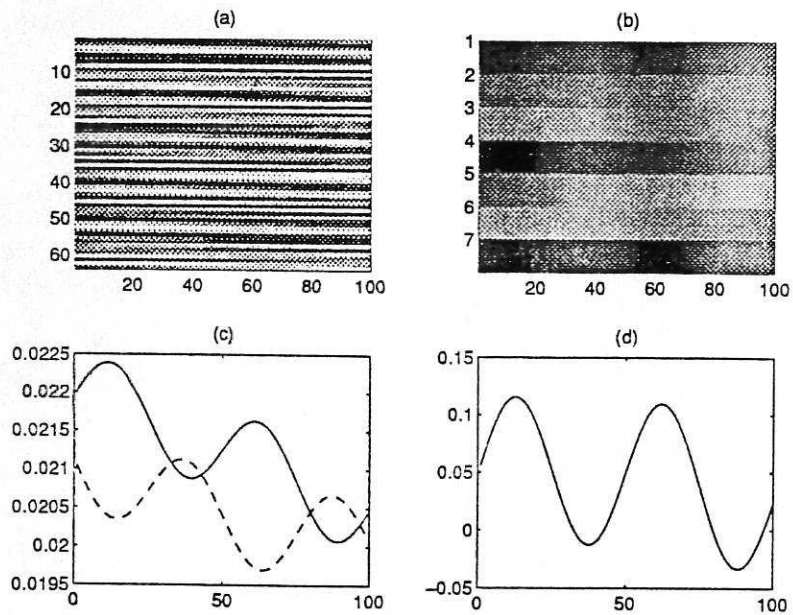


Figure 10. Experiment 4. Isobestic illumination. (570nm)



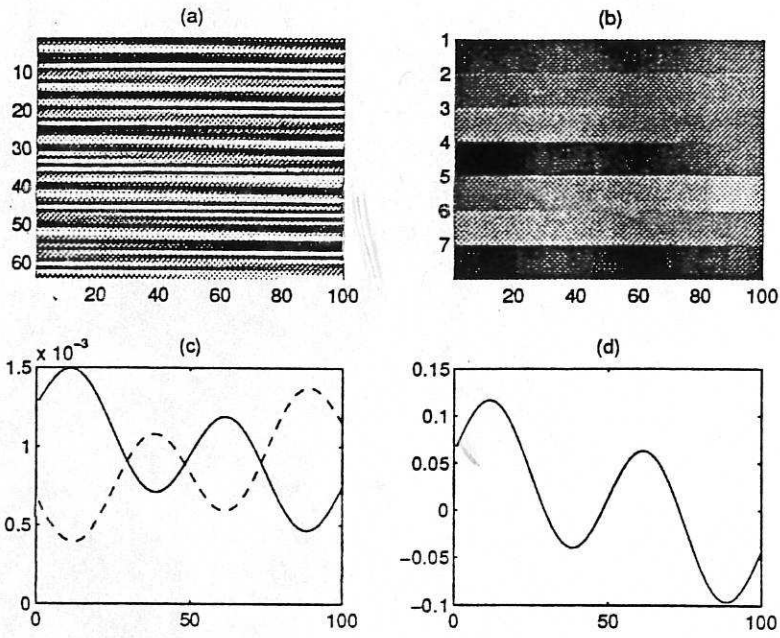


Figure 11. Experiment 5. First frame analysis with V-signal amplitude 1%